PLATES

→ indicates stratigraphic top of thin sections

Photography by Mr. W. C. Laurijssen

PLATE I

Fig. 1. Completely cemented algal-bound lime packstone overgrown by a stromatolite. f-crumbly fractures cut off at the overgrown surface. LSW 17, southern flank of Lois Syncline West. Negative print of thin section.

Fig. 2. Detail of Fig. 1. Pores and crumbly fracture filled with pore-filling calcite 1b. In the lower right-hand corner a brachiopod valve with a fibrous crust of pore-filling calcite 1a is transected by crumbly fracture f. See also Fig. 4.

Fig. 3. Clotted or "grumeleuse" texture as a result of calcitization of zoned dolomite crystals. In the pore-filling calcite 1b of the crumbly fracture at the left, the outlines of the dolomite crystals have been preserved as ferric-oxide ghosts because the regenerated pore-filling calcite crystals are large. Regeneration of the micrite mosaic obliterates the outlines and zones of the dolomite crystals and a clotty texture results. The right half of the picture shows a sharp-edged fracture cutting through the original dolomite mosaic. There are no ghosts of dolomite crystals in its pore-filling calcite generation 2. LSW 24.

Fig. 4. A second brachiopod valve (b) from thin section LSW 17 with a fibrous crust of pore-filling calcite 1a. The pseudostromatic micrite (m), surrounding the constructed void into which the fibrous crust has grown, is not lined with a similar crust. The remainder of the constructed void is filled with pore-filling calcite 1b. LSW 17, southern flank of Lois Syncline West. Phase-contrast.

Fig. 5. Algal-bound lime wackestone with a pore network (black) of constructed voids and pore-fill fossil molds connected by crumbly fractures. Internal sediments in dasycladacean mold (i_1) and in pore network (i_2) form floors. LSW 26. Negative print of thin section.

Fig. 6. Algal-bound lime packstone resembling a recrystallized recent crusty flake. The algal-bound originally micrite matrix is now mainly pseudosparitic. oq-ooid with quartz grain nucleus; o-ooid; of-ooid transected by a crumbly fracture; relicts of the ooid lamination have been preserved in the pseudospar of the crumbly fracture; e-echinoderm fragment with oncolitic algal coating; s-polyaxial sponge needle with algal coating. LSW 28.

Fig. 7. Algal-bound lime packstone. a-*Archaeolithophyllum* sp. encrusting and binding mechanically deposited wackestone compressed into packstone with parallel solution stringers (s); p-pseudostromata in sheltered places beneath the algal plates; o-ooids with a quartz grain nucleus bound together by an algal coating. LSW 29.

Fig. 8. Local intergrowth in situ of *Archaeolithophyllum* sp. (a) surrounded by pseudostromata. d-desiccation or syneresis cracks in pseudostromata; c-constructed void with internal sediment; m-pore-fill fossil mold (see also Plate II, Fig. 1). LSW 32.

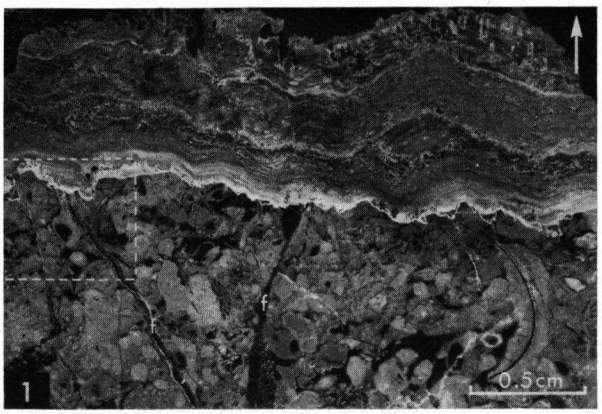
f
f
0.5 cm
1

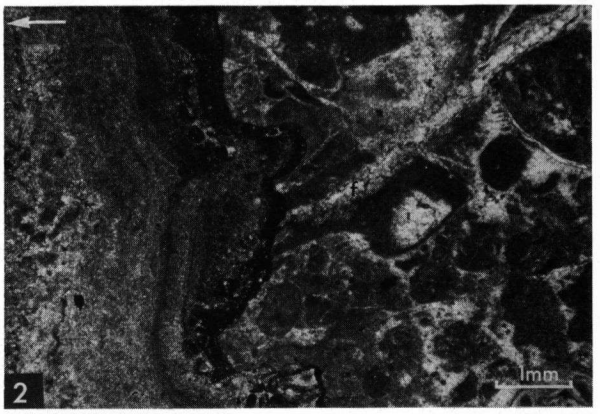
1mm
2

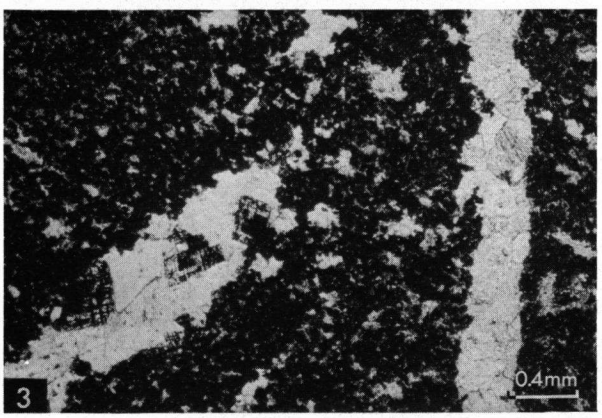
0.4mm
3

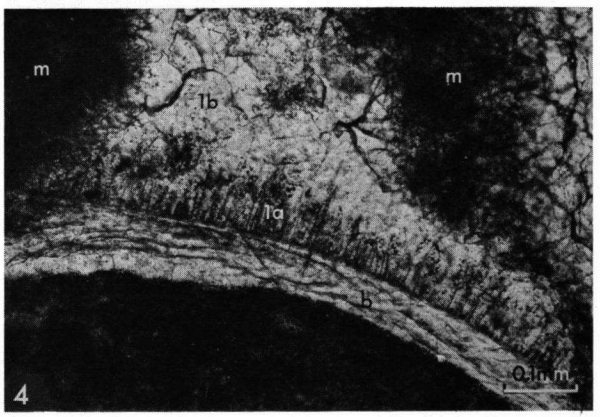
m
1b
m
1a
b
0.1mm
4

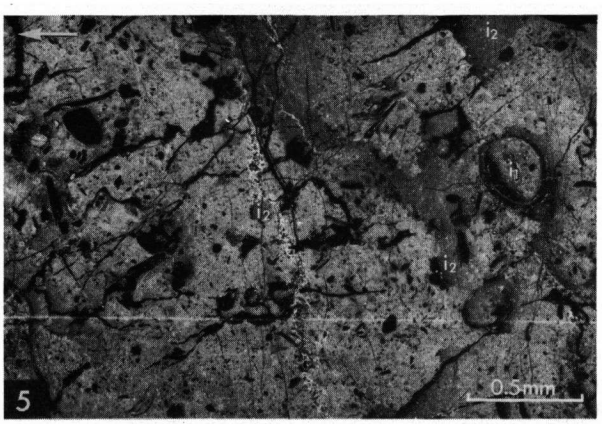
i2
i1
i2
i2
0.5mm
5

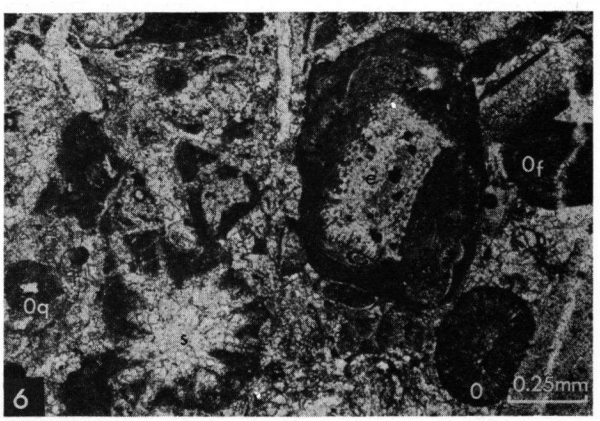
Of
Oq
s
0
0.25mm
6

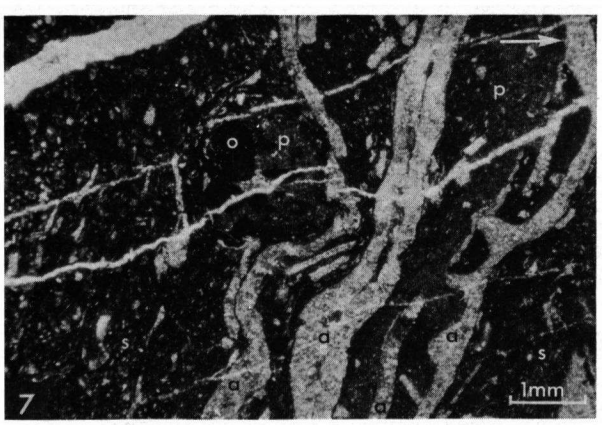
p
o
p
s
a
a
a
a
s
1mm
7

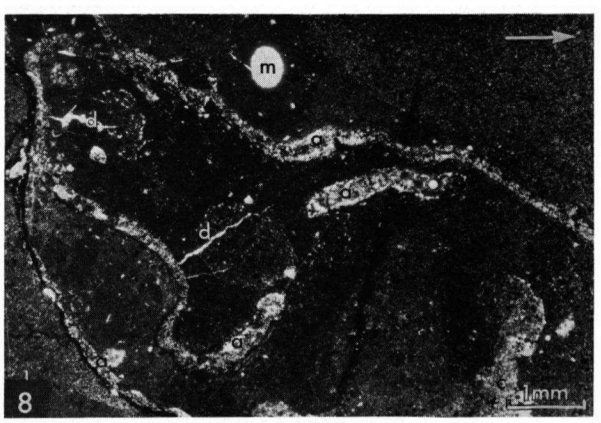
m
d
a
d
a
a
a
1mm
8

PLATE II

Fig. 1. Detail of Plate I, Fig. 8. a-*Archaeolithophyllum* sp., micritized, dolomitized, silicified and calcitized in that order; d-desiccation or syneresis cracks in pseudostromata. LSW 32.

Fig. 2. Sphinctozoan calcareous sponge (s) with floors of internal sediment and *Archaeolithophyllum missouriensum* (am) in situ. Around these in situ growths the mechanically deposited wackestone with fragments of bryozoans (b) and *Archaeolithophyllum missouriensum* (a) is draped and compressed into a packstone. LSW 33/2.

Fig. 3.a-*Archaeolithophyllum* sp.; two horizontal specimens and a vertical one broken by compaction pressure. In the dark micritized parts relicts of the hypothallus cells are visible. Parallel solution stringers intermediate between normal solution stringers and stylolites are clearly visible in the specimens of *Archaeolithophyllum* (see the section "voidless solution"); p-packstone in exceedingly close packing resulting from compaction pressure; ps-pseudostromata lacking compaction. LSW 34.

Fig. 4. Detail of another part of the thin section of Fig. 3, showing intermediate solution stringers (is), dark micritized parts (m) of *Archaeolithophyllum* with relicts of the hypothallus cells, pseudostromata (ps) lacking compaction and solution stringers (s) parallel to the bedding. LSW 34.

Fig. 5. Algal mat-like pseudostromata with algal grains (g), algal pellets and constructed voids (c), in the interstices of a skeletal framework formed by *Archaeolithophyllum* (a). Two "algal mats", lacking compaction are separated by a mechanically deposited micrite (m) with solution stringers. h-hypothallus cells. LSW 35.

Fig. 6. Detail of Fig. 5.

Fig. 7. Exceedingly close packing of ooids. Pressure solution along embayed contacts (see the sections "relation to underlying and overlying sandstones" and "voidless solution"). LSW 37.

Fig. 8. Three microstructural layers of a gastropod fragment, showing micritization and neomorphism. LSW 37. Phase-contrast.

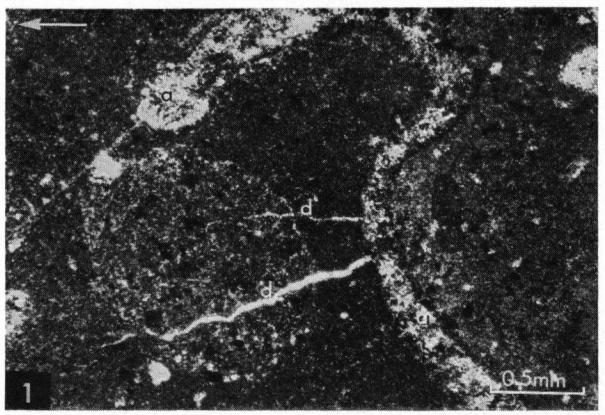
a
d'
d
a'
0.5mm
1

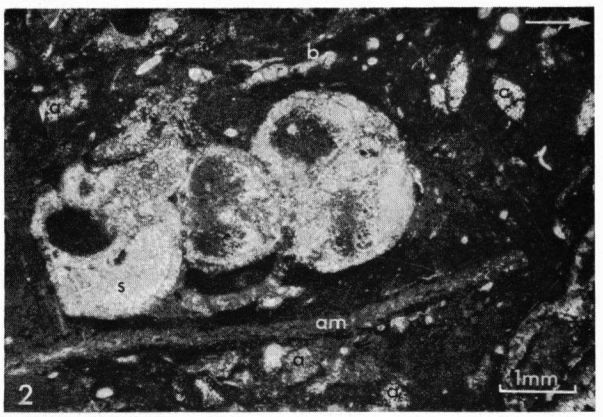
b
a
a
s
am
a
a
1mm
2


p
a
a
ps
a
1mm
3

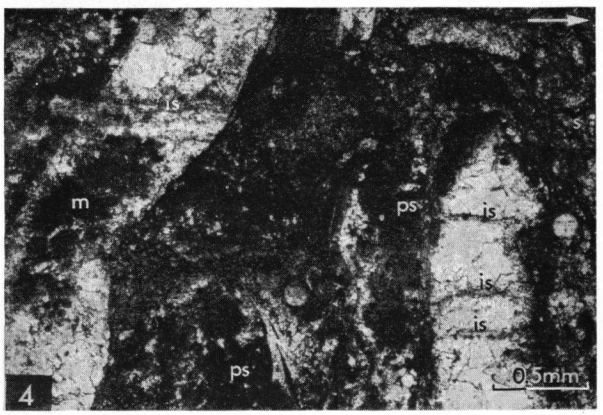
is
s
m
ps
is
is
is
ps
0.5mm
4

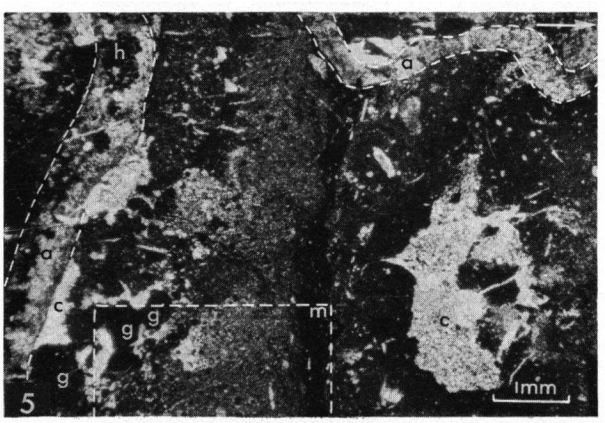
h
a
a
c
g
g
m
g
c
1mm
5

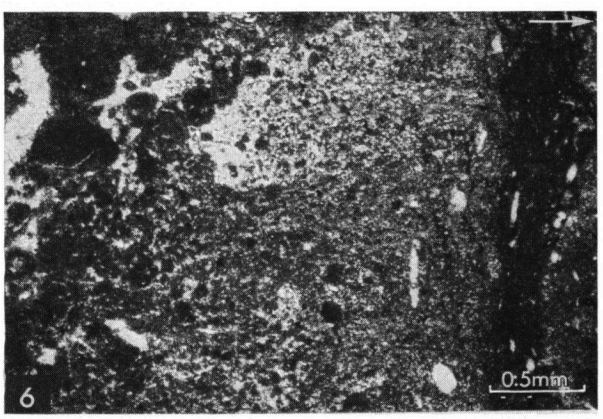
0.5mm
6

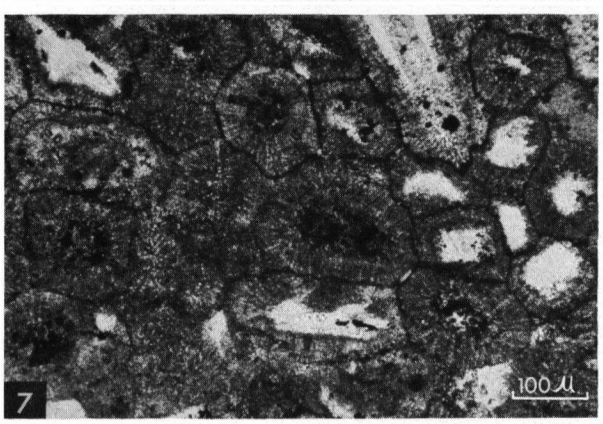
100 μ
7


1
2
3
100 μ
8

PLATE III

Fig. 1. ps-pseudostromatic micrite; c-constructed void; i-internal sediment (pelletous micrite). LSW 40.

Fig. 2. a-algal-coated pore-fill algal mold; am-algal-coated algal mold resulting from complete micritization of a calcareous Alga; b-bryozoan fragment; g-algal grains difficult to distinguish from the pseudostromatic micrite matrix (ps); o-ooids; oq-ooid with quartz grain nucleus; q-algal-coated quartz grains, some of which show partial replacement by algal micrite. LSW 42.

Fig. 3. Intergrowth of a dasycladacean (d), a bryozoan (b) and *Archaeolithophyllum missouriensum* (a). LSW 43.

Fig. 4. Intergrowth framework of *Archaeolithophyllum missouriensum* (a). In the interstices pseudostromata (ps) lack compaction. A mechanically deposited wackestone patch shows pressure solution stringers (s). Fractures in *Archaeolithophyllum* (a) and a crushed bivalved brachiopod (b) in the lower part of the picture also indicate compaction. br-bryozoan fragment. LSW 44.

Fig. 5. Development of pseudostromata (ps), lacking compaction, in a protected niche under an *Archaeolithophyllum* intergrowth. Above and beneath are wackestone patches (w) with pressure solution stringers. b-brachiopod valve; br-bryozoan fragment. LSW 44.

Fig. 6. A brachiopod shell on top of an algal mat (m), partly in overlying pseudostromatic micrite (ps) and partly in a solution void (s). The pseudostromatic micrite and the algal mat resisted compaction. The compaction pressure was conducted to the right half of the brachiopod shell with the result that the anterior part of the brachiopod was "squeezed out". The fracturing by compaction took place before consolidation of the internal sediment which consequently adjusted its level to the new horizontal and before filling with calcite generation 1b which is evident from its optical continuity around the broken parts of the valves, see Figs. 7 and 8. LSW 47.

Fig. 7. Detail of Fig. 6; × nicols.

Fig. 8. Detail of Fig. 6; // nicols.

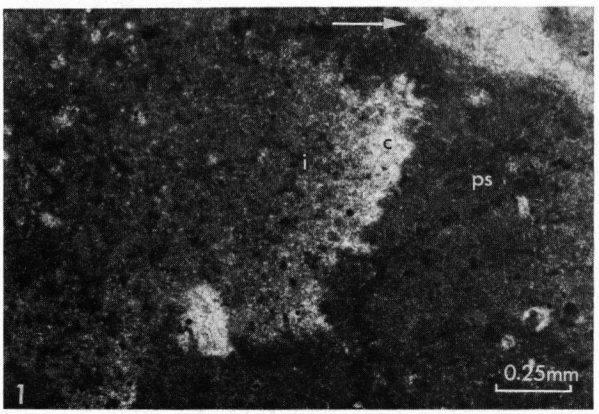
i
c
ps
0.25mm
1

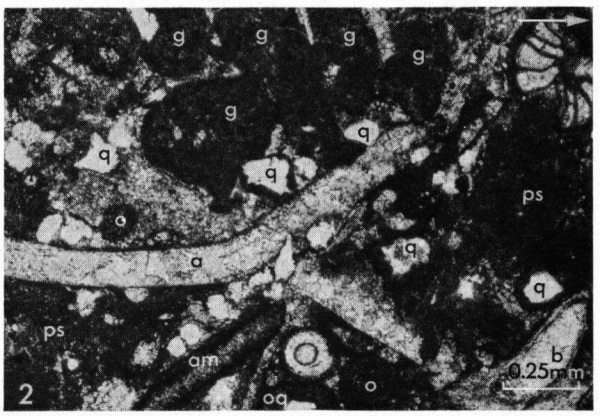
g
q
a
ps
am
og
o
b
0.25mm
2

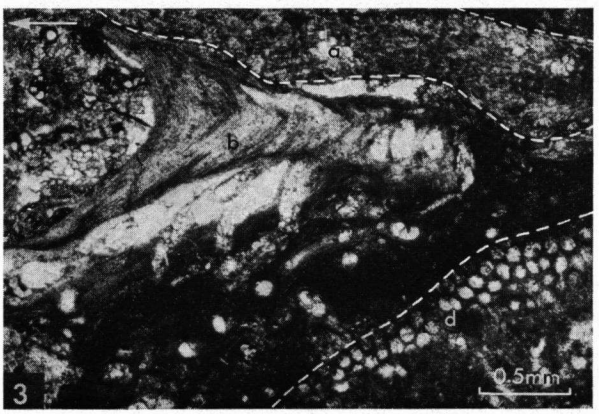
a
b
d
0.5mm
3


s
a
ps
br
b
1mm
4

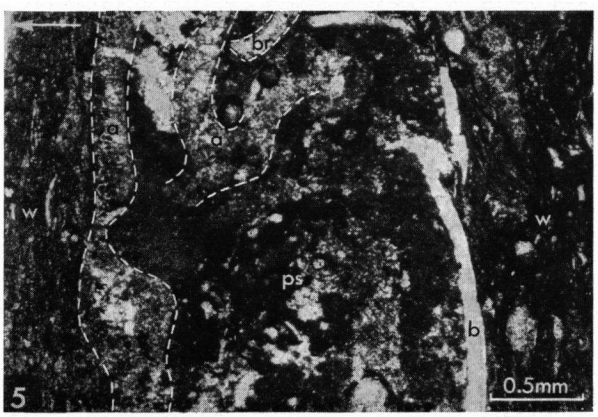
br
a
w
ps
b
0.5mm
5

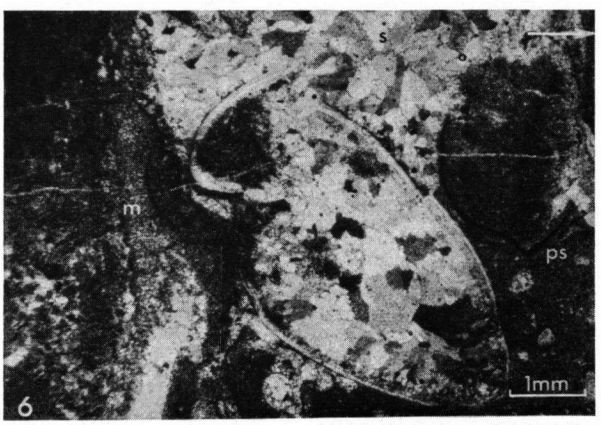
s
m
ps
1mm
6

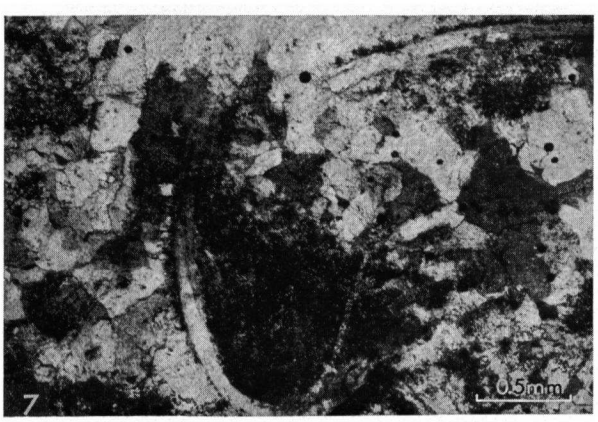
0.5mm
7

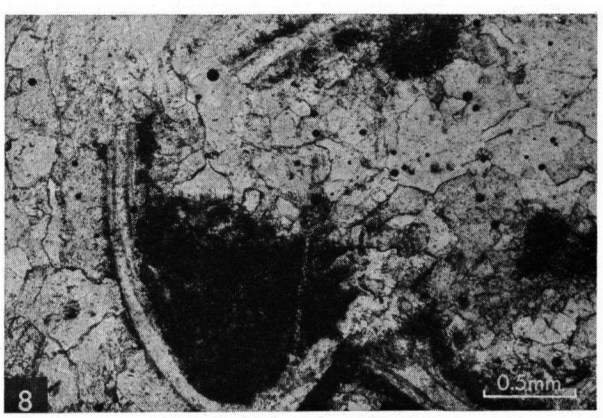
0.5mm
8

PLATE IV

Fig. 1. Sharp-edged fracture transecting a mosaic of dolomitized micrite and pseudospar. Dolomite rhombs in pseudospar are larger and more translucent. LSW 51.

Fig. 2. Detail of Fig. 1. A single dolomite rhomb developed in the pore-filling calcite of the sharp-edged fracture.

Fig. 3. Constructed void (c) with fibrous crust of pore-filling calcite generation 1a, transected by a short crumbly fracture. Solution voids (s) with pore-filling calcite generation 1b and neomorphic calcite (neomorphic calcite creating solution). LSW 52. × nicols.

Fig. 4. Detail of Fig. 3. The internal sediment was cemented by pore-filling calcite generation 1a. n-neomorphic calcite (neomorphic micrite and pseudospar) of the solution voids.

Fig. 5. Algal-bound dolo-packstone, interpreted as a dolomitized crusty flake. Micrite inclusions in the dolomite crystals still show a patchy distribution. Algal-coated quartz grains, algal pellets and algal-coated dolomitized fossil molds (m) around a micritized and aggrading neomorphic pelecypod valve (p) with relicts of the microstructure. b-valve fragment of a brachiopod. See also Pl. V, Figs. 1 and 2. LSW 56.

Fig. 6. Neomorphic gastropod with completely dolomitized internal sediment (i). 1-pore-filling calcite, selectively dolomitized around inclusions of an internal algal micrite coating; 2-dolomite cement; 3-calcite filling remaining pore space (see the section "dolomite cement"). LSW 56.

Fig. 7. Detail of Fig. 6.

Fig. 8. Almost completely dolomitized neomorphic skeletons of gastropods (see the section "dolomite replacing bioclasts"). LSW 56.

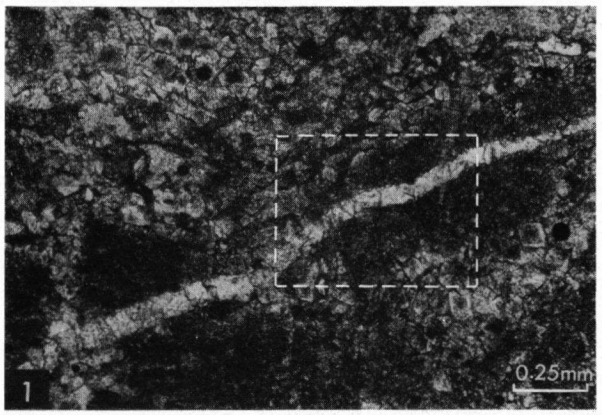
0.25mm

1

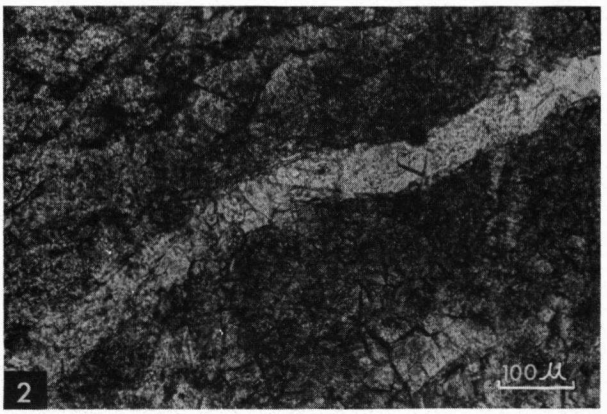
100 μ

2

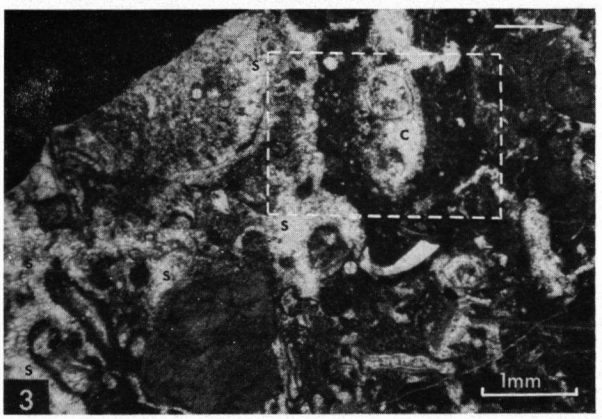
s
c
s
s
s
1mm

3

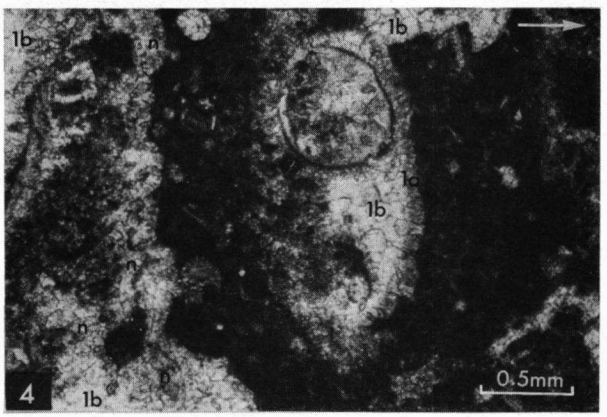
1b
n
1b
1a
1b
n
p
p
1b
0.5mm

4

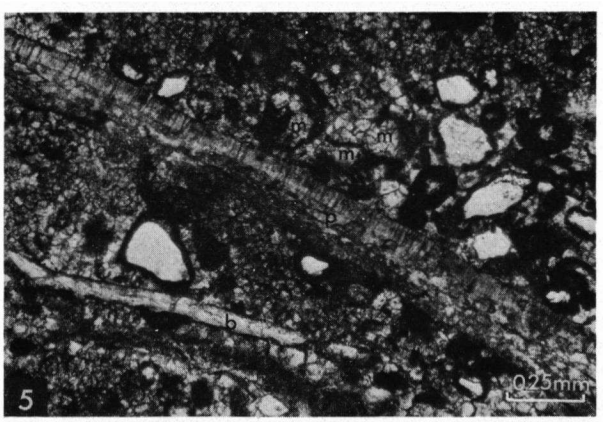
m
m
p
b
0.25mm

5

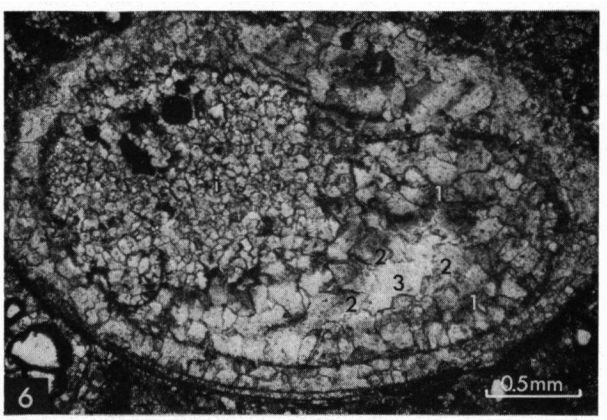
1
2
3
2
2
1
0.5mm

6

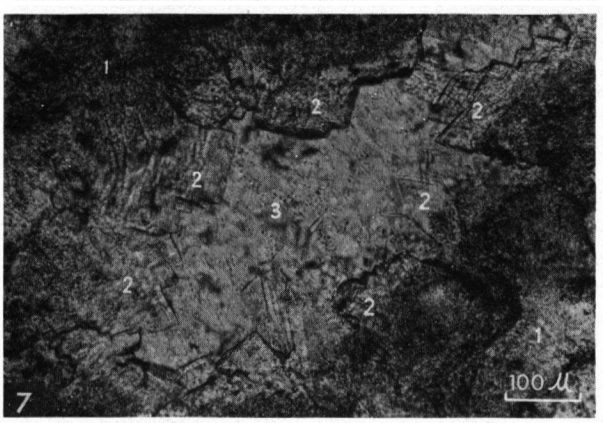
1
2
2
2
3
2
2
2
1
100 μ

7

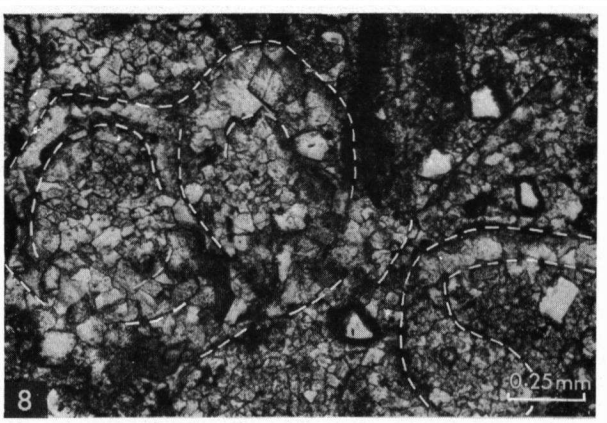
0.25mm

8

PLATE V

Fig. 1. Detail of Pl. IV, Fig. 5. Micritization and subsequent aggrading neomorphism of a pelecypod valve. The prismatic layer (p) of the microstructure has been preserved. Matrix of dolomite crystals with micrite inclusions and linings of black organic streaks. LSW 56. Phase-contrast.

Fig. 2. Detail of Fig. 1 showing micrite inclusions in the neomorphic calcite crystals and in the preserved original prismatic crystals of the pelecypod valve. Algal-coated quartz grain shows projections of algal micrite (arrows), replacing the quartz. Phase-contrast.

Fig. 3. Local intergrowth in situ of colonies of loosely arranged calcareous algal tubes intimately associated with pseudostromata. Desiccation or syneresis cracks rise vertically from the surface of the calcareous algal tubes which did not follow the shrinking of the surrounding dark pseudostromatic body. LSW 63.

Fig. 4. Detail of Fig. 3.

Fig. 5. In situ growth of calcareous algal tubes contrary to gravity over a pseudostromatic body (ps). LSW 63.

Fig. 6. Oncolite around a codiacean Alga as a nucleus. The outline of the oncolite is not always distinct because of local integration with the pseudostromatic matrix of the algal-bound lime packstone. LSW 64.

Fig. 7. Detail of the same thin section of Fig. 6 showing algal-coated neomorphic fossil molds difficult to distinguish from the neomorphic matrix. The algal coatings show integration with the matrix. c-mold of a micritized codiacean Alga with a heavy algal coating.

Fig. 8. Detail of Fig. 7. In the upper left-hand corner solution stringers (s) indicate local compaction. m-algal-coated neomorphic fossil molds.

1

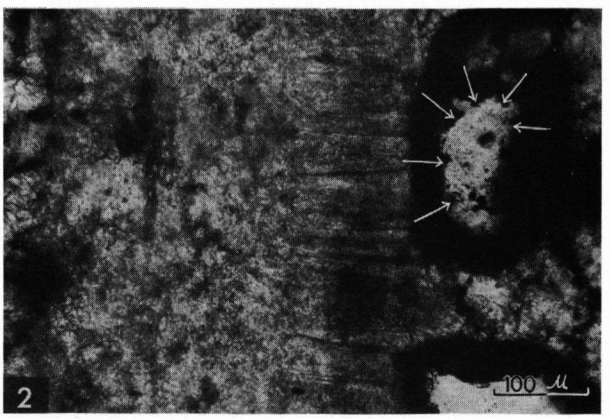

2

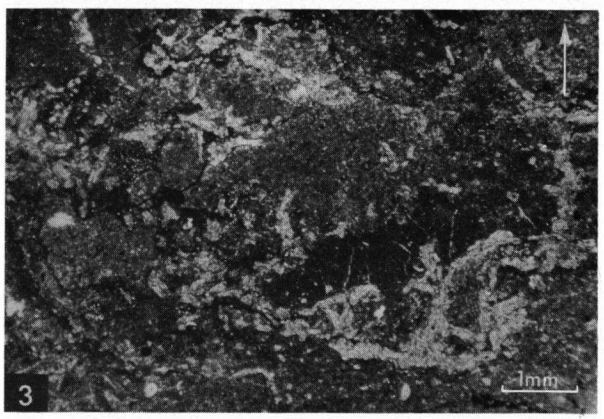

3

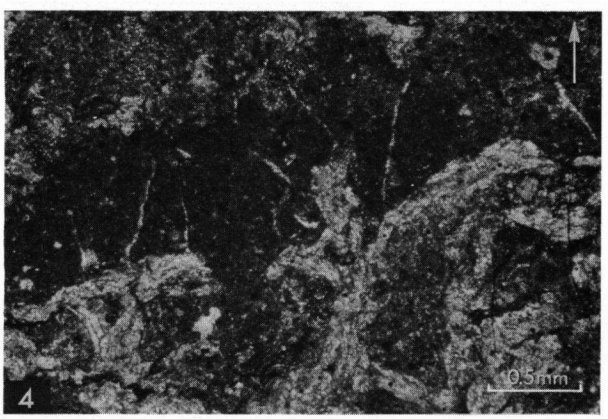

4

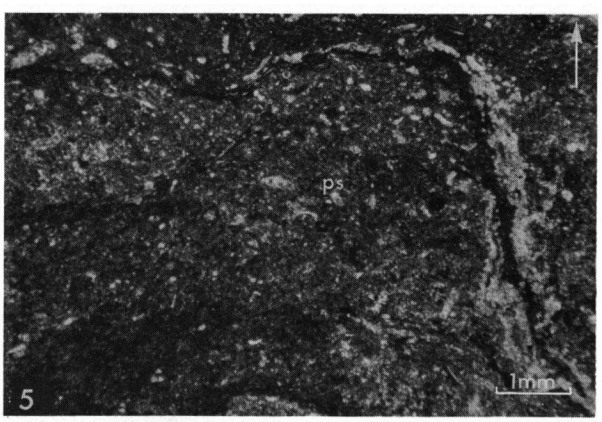

5

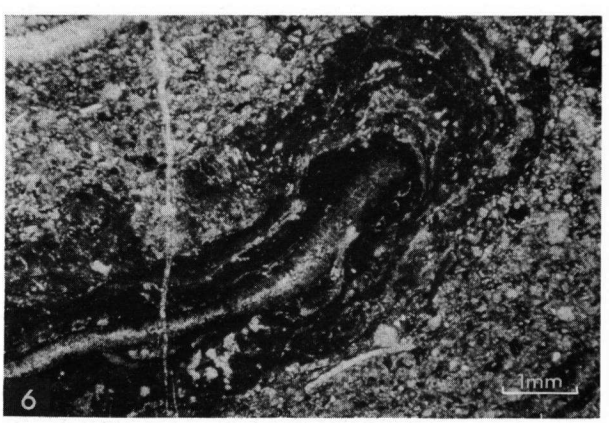

6

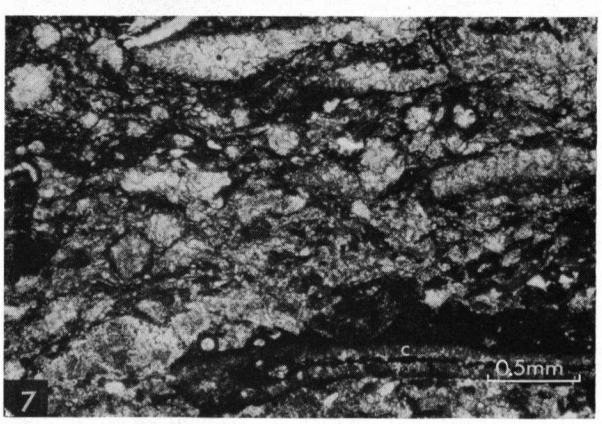

7

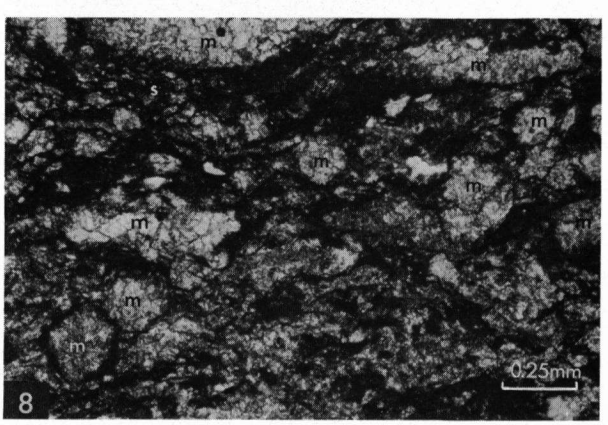

8

PLATE VI

Fig. 1. Algal pore-fill molds (m) with algal coatings and undissolved micritized remnants. cr-crumbly fracture with a mosaic of pore-filling calcite 1b which is integrated with the mosaic of pore-filling calcite 1b of a solution void (s). f_1-sharp-edged fracture transecting the crumbly fracture (cr) and itself transected by a younger set of parallel sharp-edged fractures (f_2). c-constructed voids, probably somewhat enlarged by dissolution. p-pelletous pseudostromatic micrite. LSW 67.

Fig. 2. Crumbly fracture (cr) with pseudospar "transecting" a fossil. The skeletal outline of the fossil can be traced in the peudospar of the crumbly fracture (arrows). The internal sediment in the fossil recrystallized along the "transection" (see the section "pseudospar in relation to fractures"). LSW 69.

Fig. 3. Patch of pseudospar (ps) in connection with crumbly fracture (cr) (see the sections "pseudospar in relation to fractures" and "neomorphic calcite creating solution"). LSW 69.

Fig. 4. Remnants of a micritized algal mold internally and externally coated by a dark pseudostromatic algal coating in which calcareous algal tubes are embedded. The void within the algal mold is filled with pelletous internal sediment and roofed over by the same pseudostromatic micrite of the algal coating; a fossil fragment (f) was tightly bound within the roof and did not fall. LSW 69.

Fig. 5. Algal-bound lime packstone with in situ growth of *Archaeolithophyllum* sp. (a), local intergrowth (i) in situ of *Archaeolithophyllum* sp. and calcareous algal tubes embedded in pseudostromata. o-oncolite around a codiacean Alga; g-gastropod with internal sediment; b-brachiopod with floor of internal sediment; n-patch of neomorphic calcite created by solution. Several Foraminifora, *Bradyina* sp. (br), are present which are rather large but still belong to the group of smaller Foraminifera. LSW 72. Negative print of thin section.

Fig. 6. Detail of the intergrowth (i) of Fig. 5. a-micritized and aggraded neomorphic *Archaeolithophyllum;* t-calcareous algal tubes embedded in the pseudostromatic body (black); d-desiccation or syneresis cracks connecting constructed voids; al-allochems "floating" in pseudospar created by solution; c-clear pore-filling calcite in solution voids.

Fig. 7. Detail of the oncolite (o) of Fig. 5. Locally the pseudostromatic algal coating of the oncolite is integrated with the pseudostromatic matrix of the algal-bound lime packstone, for instance around a void (v) which might be a pore-fill fossil mold or a constructed void.

Fig. 8. The neomorphic matrix of the algal-bound lime packstone LSW 72. Smaller Foraminifera and algal pellets "float" in pseudospar and neomorphic micrite. Phase-contrast.

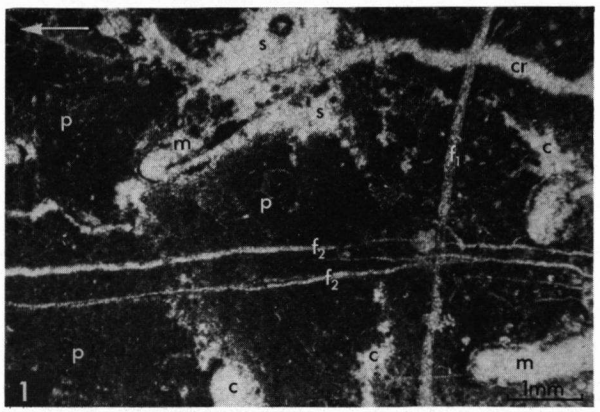
s
cr
p
s
m
f_1
c
p
f_2
f_2
p
c
m
c
1mm
1

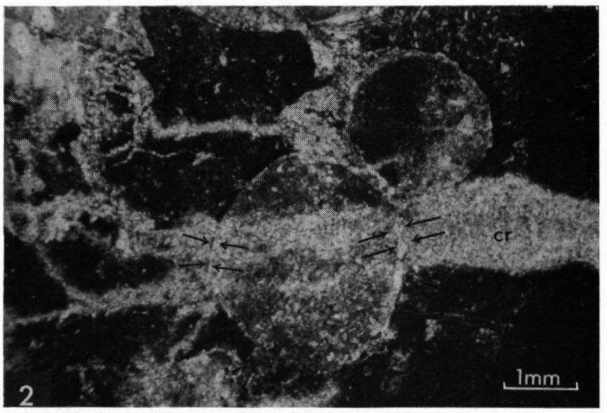
cr
1mm
2

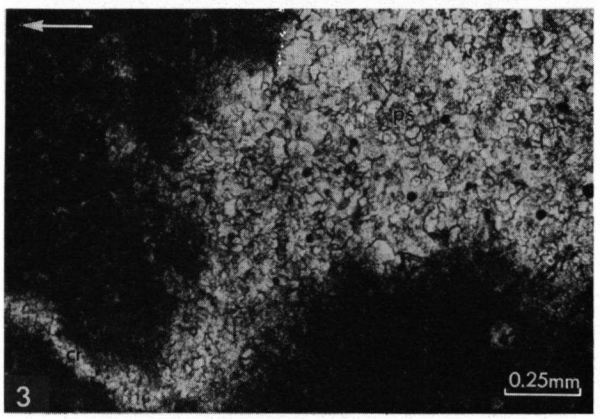
ps
cr
0.25mm
3

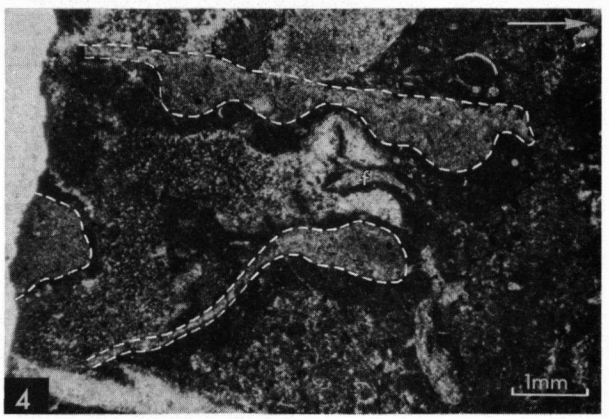
1mm
4

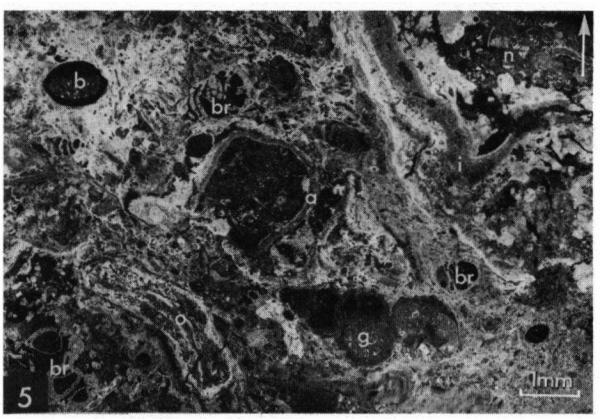
b
br
n
i
a
br
o
g
br
1mm
5

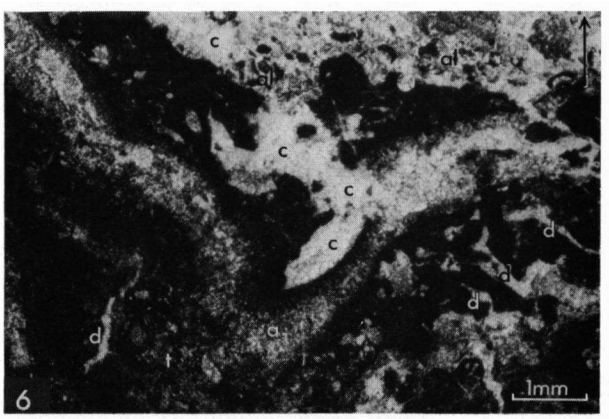
c
al
al
c
c
c
d
d
d
d
a
1mm
6

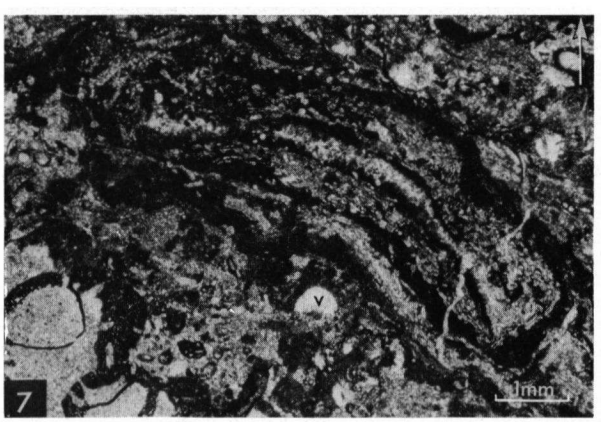
v
1mm
7

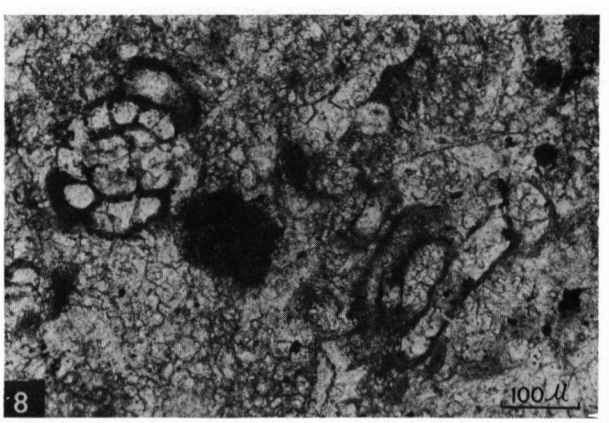
100 μ
8

PLATE VII

Fig. 1. Internal sediment of brachiopod (b) of Pl. VI, Fig. 5. Micritized small bioclasts and algal pellets in neomorphic micrite, pseudospar and euhedral dolomite crystals (see the section "internal sediment"). LSW 72. Phase-contrast.

Fig. 2. Solution phenomena in internal sediment of gastropod (g) of Pl. VI, Fig. 5. Remnants of internal sediment (r) are preserved in the midst of pore-filling calcite. Solution also affected the wall of the gastropod (arrow). For more detail see Figs. 4, 6, and 8. LSW 72.

Fig. 3. Brachiopod in a pseudostromatic micrite, similar to mechanically deposited micrite. The pseudostromatic nature is indicated by the roof (r) over the intrabrachiopod void. The internal algal coating and irregular pseudostromatic filling of the brachiopod are also suggestive of algal-bound micrite. i-floors of internal sediment. LSW 73.

Figs. 4 and 6. These pictures together show the part of the wall indicated in Fig. 2. Dissolution of the micritized and neomorphic gastropod wall is clearly visible (arrow in Fig. 4); its place is now occupied by pore-filling calcite (p). In the neomorphic gastropod wall relicts of several microstructural layers are visible. The mosaic of neomorphic calcite of the internal sediment continues locally in a microstructural layer of the gastropod wall. This is interpreted as aggrading neomorphism of heavily micritized parts of the skeleton (see also Fig. 8). Phase-contrast.

Fig. 5. Algal-bound lime packstone. m-neomorphic molds of calcareous Algae, coated with dark algal micrite and calcareous algal tubes; g-algal grains; e-echinoid plate with tubercle; o-small oncolites, the one at the right is an intergrowth of two oncolites, one around a bryozoan fragment (b) and one with a void, probably a pore-fill fossil mold, filled with algal grains, algal pellets and pore-filling calcite.

Fig. 6. see Fig. 4.

Fig. 7. Detail of Fig. 5. m-neomorphic algal molds; r-relicts of hypothallus cells of *Archaeolithophyllum;* g-algal grains; e-embayed contacts: e_1 between an algal mold and an algal coating, e_2 between algal molds and an algal grain. o-part of the intergrown oncolite of Fig. 5.

Fig. 8. Detail of the part of the gastropod wall indicated in Fig. 6. Phase-contrast.

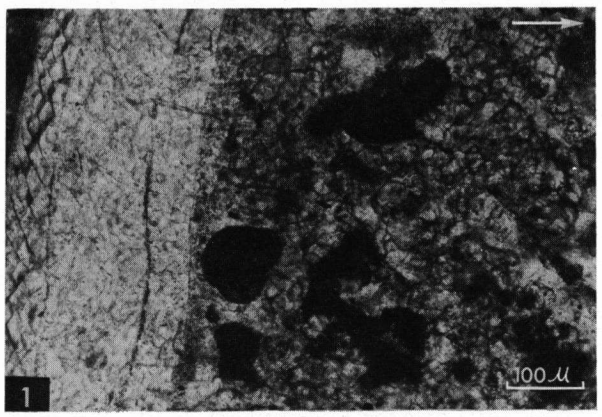
100 μ

1

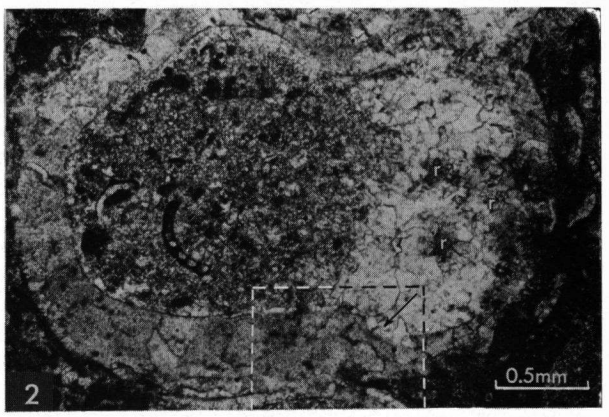
r
r
0.5mm

2


r
1mm

3


p
p
p
p
p
100 μ

4

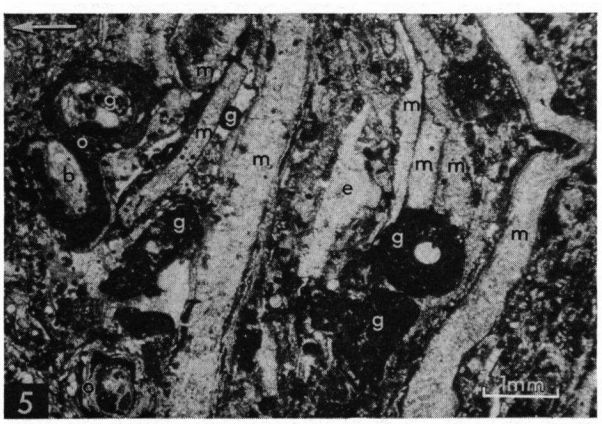
m
g
o
b
e
1mm

5

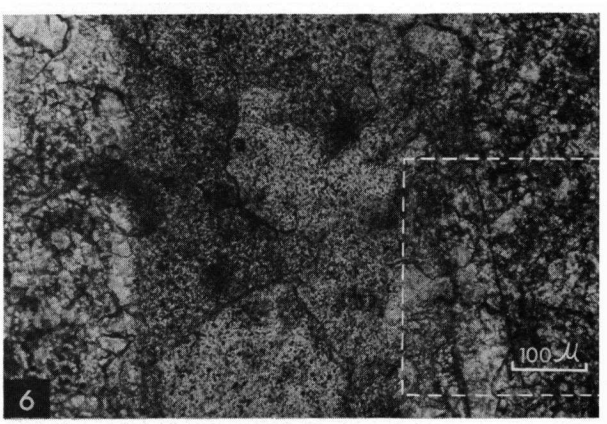
100 μ

6

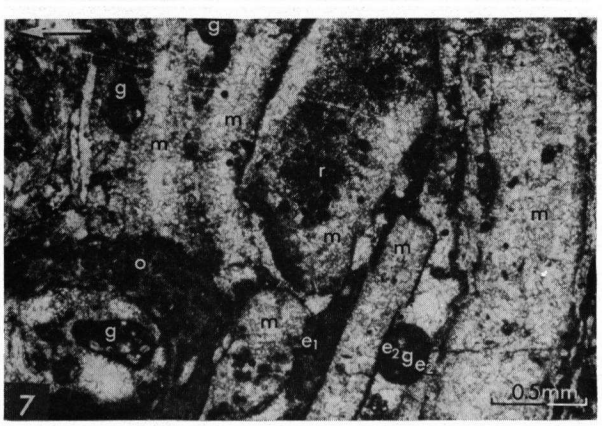
g
m
r
o
e1
e2 g e2
0.5mm

7

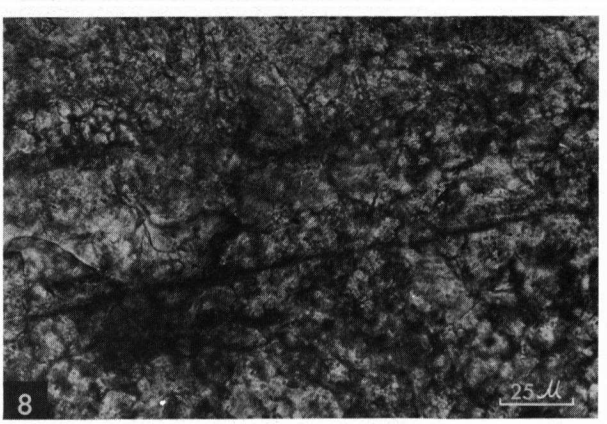
25 μ

8

PLATE VIII

Fig. 1. Algal pellets formed by algal coating of small allochems. The algal coatings are partly neomorphic: neomorphic fibrous spherulitic micrite to fibrous spherulitic pseudospar (see the section "pseudospar"). LSW 80.

Fig. 2. Intergrowth in situ of *Archaeolithophyllum* pore-fill molds (a), fenestrate bryozoans (b) and pseudostromata (white). A gastropod, probably browsing in the pseudostromatic algal envelope, became entangled in the algal mass and was incorporated in the intergrowth. The algal pellets surrounding the intergrowth most probably were entrapped and bound by freely waving algal filaments (see Fig. 4.). 3-detail see below; 4-detail see below; 5-detail see below; 6-detail see below. LSW 82. Negative print of thin section.

Fig. 3. Detail 3 of Fig. 2. Undissolved micritized remnant of *Archaeolithophyllum*. a-algal pore-fill mold; c-constructed voids in the pseudostromatic envelope; h-hypothallus cells, still vaguely visible.

Fig. 4. Detail 4 of Fig. 2. Externally calcified remnants of the non-calcareous algal filaments which probably trapped and bound the algal pellets. v-void beneath the intergrowth filled with pore-filling calcite 1b; b-fenestrate bryozoan.

Fig. 5. Detail 5 of Fig. 2. Crumbly fracture (f) in pseudostromatic envelope connects the void (v) beneath the intergrowth, the inter-allochem pores and the void of the dissolved *Archaeolithophyllum* (a). This pore network has been filled with pore-filling calcite 1b. The void of the dissolved *Archaeolithophyllum* is lined with undissolved micritized skeletal remnants; just beneath the entrance of the crumbly fracture is a floor of internal sediment.

Fig. 6. Detail 6 of Fig. 2. In only two places (white arrows) has the dark pseudostromatic envelope penetrated the void left after dissolution of a gastropod. This indicates the general coherent character of the algal-bound pseudostromatic micrite. The internal sediment of the gastropod has not been washed into the void altogether which indicates its rapid consolidation. Penetration of the internal sediment into the void may also have been prevented by the presence of an internal algal coating which lines the void on top of the internal sediment and shows only local interruptions (black arrows). Obviously this thin internal algal coating was coherent enough to remain preserved after dissolution of the gastropod skeleton.

Fig. 7. Algal grains (g); the left was formed by an algal coating around fossils of which only vague pore-fill molds are left; within the right one, bryozoan fragments can still be distinguished. s-pore-fill molds of spherulites. LSW 84.

Fig. 8. Echinoderm fragment with deviating microstructure. Instead of the characteristic monocrystal microstructure, this fragment shows extinction of several crystals. Conjunction of several plates? LSW 84. × nicols.

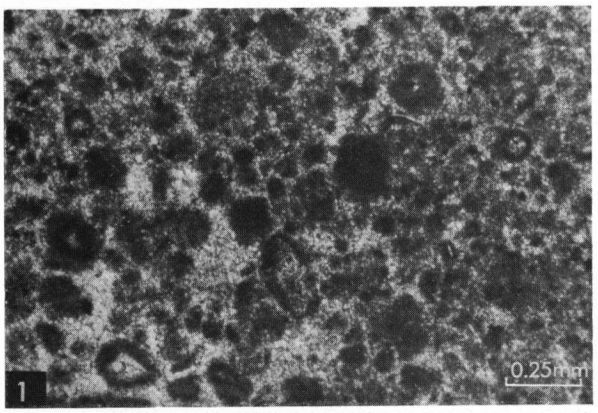
0.25mm

1

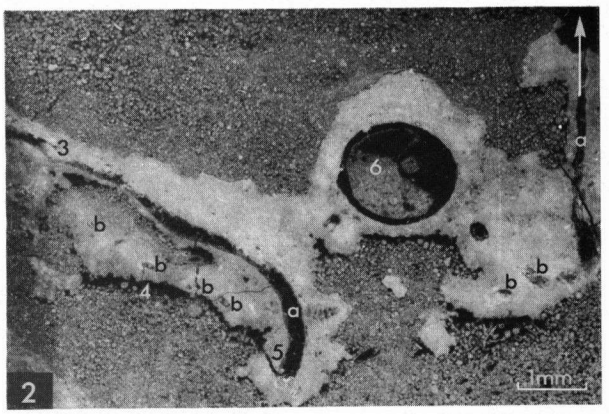
3
6
a
b
b
b
b
b
b
4
a
5
1mm

2

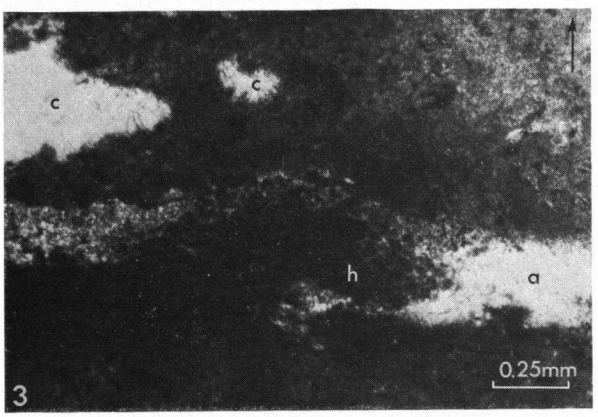
c
c
h
a
0.25mm

3

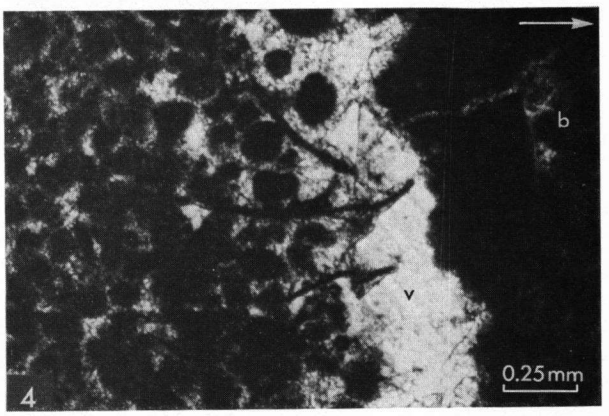
b
v
0.25mm

4

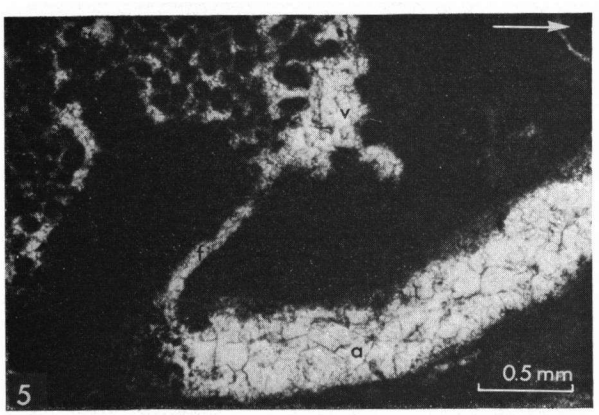
v
a
0.5mm

5

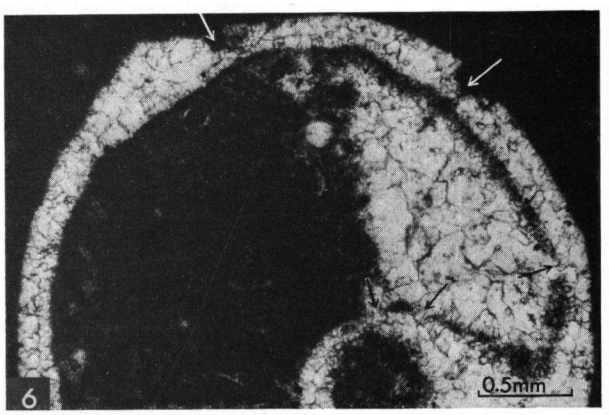
0.5mm

6

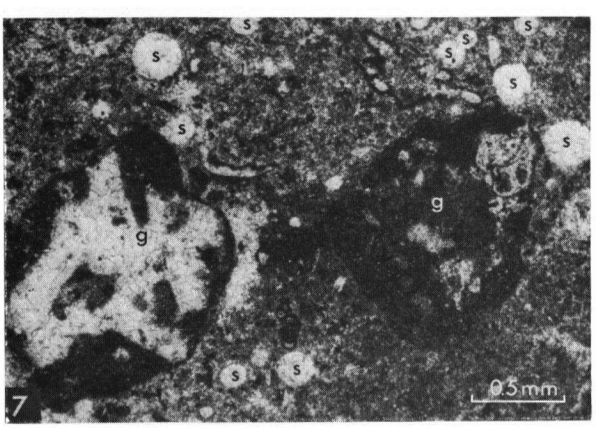
s
s
s
s
s
s
s
s
s
s
s
s
g
g
0.5mm

7

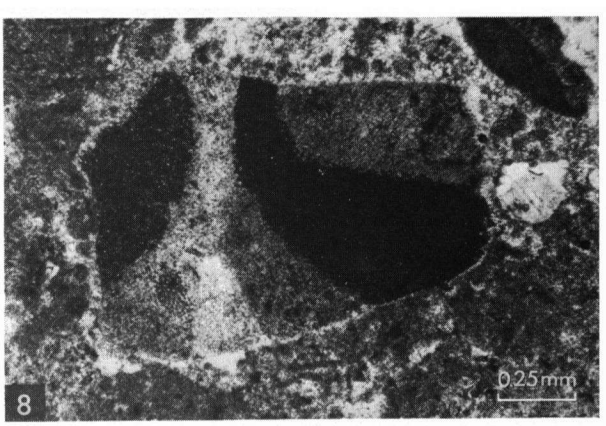
0.25mm

8

PLATE IX

Fig. 1. Algal-bound lime wackestone with local intergrowth (in) in situ of colonies of loosely arranged calcareous algal tubes and pseudostromata. In the constructed voids of this intergrowth are floors of internal sediment (i). The tightly bound pseudostromatic parts appear white in this photograph. Constructed voids, locally enlarged by solution, and pore-fill molds are black. LSW 85. Negative print of thin section.

Fig. 2. Detail of the intergrowth (in) of Fig. 1, just to the left of the upper void with internal sediment and outside the picture. c-constructed voids lined with pore-filling calcite 1a and filled with pore-filling calcite 1b. A crumbly fracture connects the voids and transects fibrous crust 1a (arrows). After crumbly fracturing some solution took place, as indicated by the partial lack of algal coating and the fibrous crust at location ×. t-calcareous algal tubes.

Fig. 3. Detail of Fig. 2 with the same symbols ×, t, 1a. Fibrous crust 1a is neomorphic; only vague relicts of fibres are visible. The internal sediment of the void consists of algal pellets and neomorphic micrite. Phase-contrast.

Fig. 4. Spherulite with algal coating. After micritization, aggrading neomorphism changed the originally fibrous spherulite into a spherical calcite crystal with NE-SW cleavage lines. The fibrous microstructure and the NdE_1 calcite of the micritization have been preserved as relicts in the monocrystal. LSW 89. Phase-contrast.

Fig. 5. A pseudostromatic body lacking compaction surrounded by mechanically deposited wackestone with parallel arrangement of fossils and with solution stringers indicating compaction. The mechanically deposited wackestone shows selective dolomitization with respect to the pseudostromatic body. Sharp-edged fractures are present in a set of parallel fractures. They are more obvious in the pseudostromatic body than in the mechanically deposited wackestone because of the different fabrics of the two depositional textures. At least three generations of sharp-edged fractures are present (1, 2, 3; arrows point to offsets of 1 by 2 and 2 by 3). LSW 91.

Fig. 6. Lens-like termination of the pelletous pseudostromatic body of Fig. 5 surrounded by solution stringers contrary to gravity. Sharp-edged fractures, well developed in the pseudostromatic body, thin out (1) or split up into several smaller ones (2) as soon as they transect the mechanically deposited wackestone. 3-sharp-edged fracture offsetting a solution stringer. The sharp-edged fracture to the left did not succeed in transecting the solution stringer. Offset of sharp-edged fractures by solution stringers has also been observed locally. The thin continuations (1) of the sharp-edged fractures in the dolomitized mechanically deposited wackestone show dolomitization of their pore-filling calcite.

Fig. 7. Branch of *Anthracoporella* broken by compaction after filling of the intrafossil void with pore-filling calcite 1b. Solution stringers in the mechanically deposited wackestone are draped around the fragment with its pore-filling calcite. Sharp-edged fractures transect the solution stringers and originated later. LSW 92.

Fig. 8. Continuation of the right branch of Fig. 7 with dark algal coating lacking compaction in contrast to the overlying mechanically deposited wackestone with solution stringers. c-constructed void in algal coating connecting with a boring(?) or solution (?) channel through the *Anthracoporella* branch. Two generations of sharp-edged fractures are present.

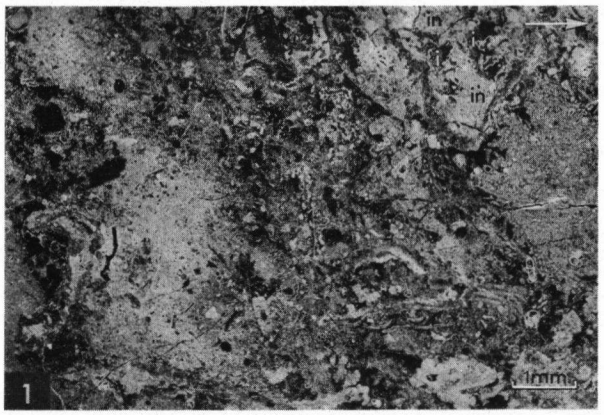
in
in
1mm
1

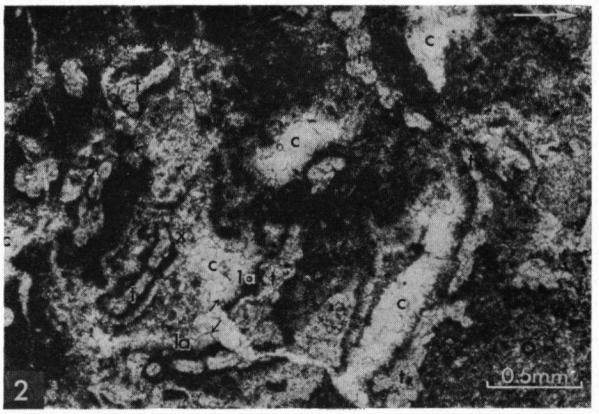
c
c
c
c
c
1a
1a
0.5mm
2

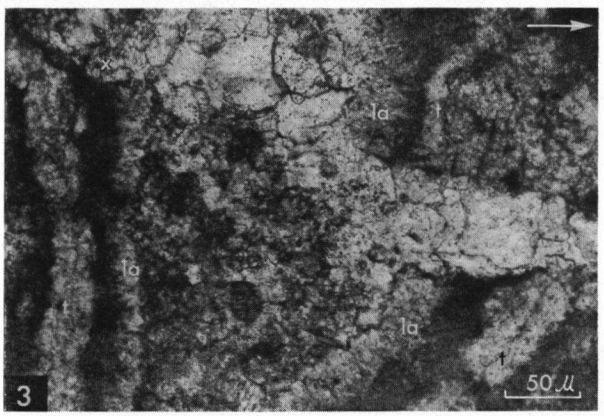
x
1a
1a
1a
50 μ
3

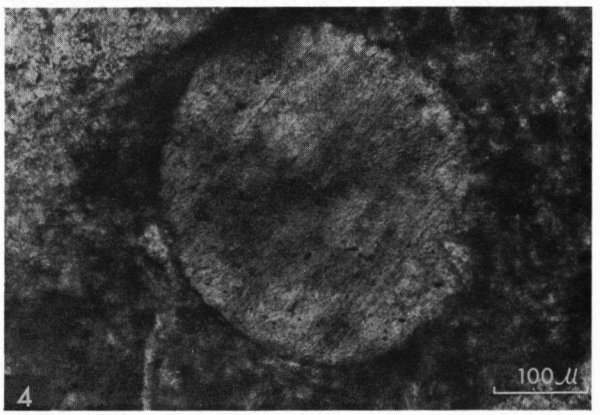
100 μ
4


1
2
3
1mm
5

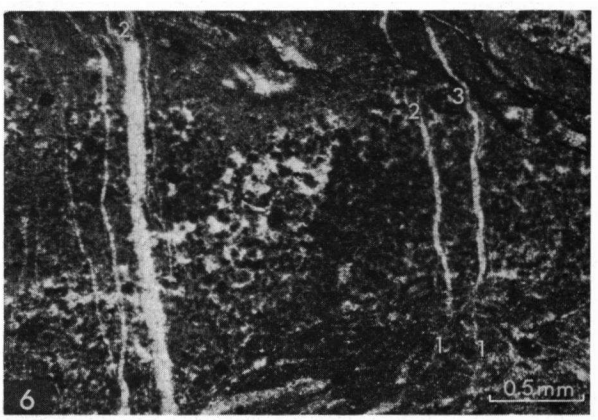
2
2
3
1
1
0.5mm
6

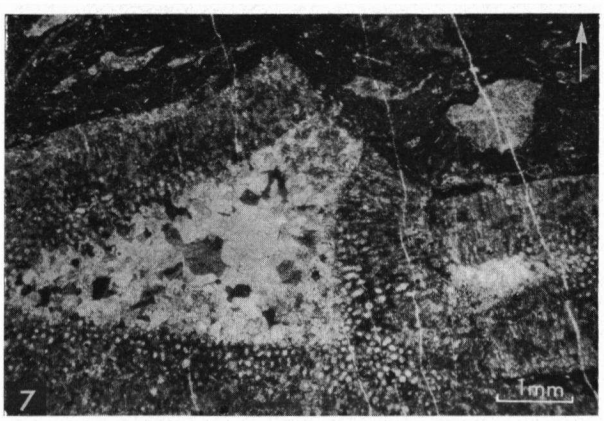
1mm
7

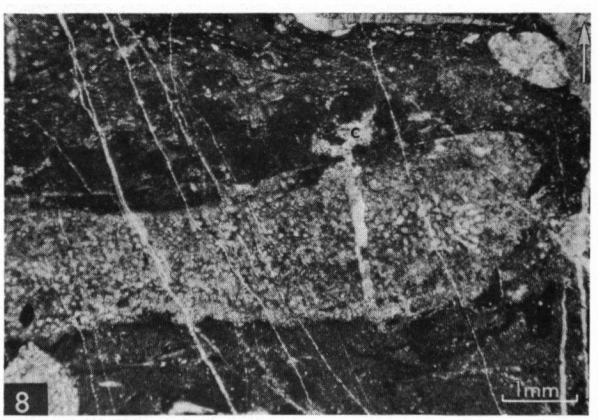
c
1mm
8

PLATE X

Fig. 1. Algal-bound lime wackestone with a local intergrowth in situ (upper right in figure). The local intergrowth is a laminated and pseudostromatic algal head coated by dark pseudostromatic micrite (white) containing bryozoans, ostracods, encrusting Foraminifera, calcareous algal tubes and an encrusting calcareous Alga *Parachaetetes* sp. LSW 94. Negative print of thin section.

Fig. 2. Detail of Fig. 1 showing the partly pseudostromatic (ps) and partly laminated (l) nature of the algal head. c-dark pseudostromatic algal coating. On the left is an algal-bound wackestone with algal pellets and algal grains (g).

Fig. 3. Detail of Fig. 2 showing obliteration of the algal mat laminations by neomorphism. Clear calcite patches (p) suggest neomorphism by impregnation of porous algal micrite by calcium carbonate-rich solutions.

Fig. 4. Fibrous quartz crystals replacing pore-filling calcite in a mold within the algal head of Fig. 1. Phase-contrast.

Fig. 5. Constructed void (v) with a floor of algal pellets in the algal-bound algal pellet and algal grain wackestone of Fig. 1. g-algal grains.

Fig. 6. Sharp-edged fracture transecting dolomite rhombs (arrows) with both centrifugal and centripetal replacement by calcite. LSW 97.

Fig. 7. Dolomite rhomb with a dark micritic center, regenerated by calcitization (centrifugal replacement). Centripetal replacement is visible in the upper corner of the rhomb; the regenerated micrite mosaic is coarser than the micrite surrounding the rhomb. Patches with high relief in the rhomb are silicified micrite inclusions (s). LSW 97. Phase-contrast.

Fig. 8. Local intergrowth in situ of colonies of calcareous algal tubes and pseudostromata. v-constructed voids enlarged by solution, indicated by partly dissolved algal tubes adjacent to the voids (arrows). i-floors of internal sediment; s-stylolite perpendicular to the bedding. LSW 101.

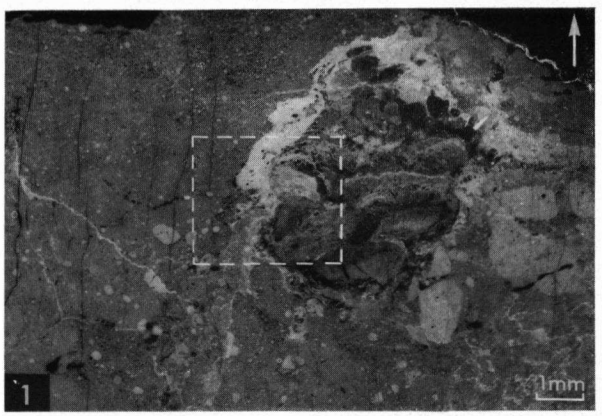
1mm

1

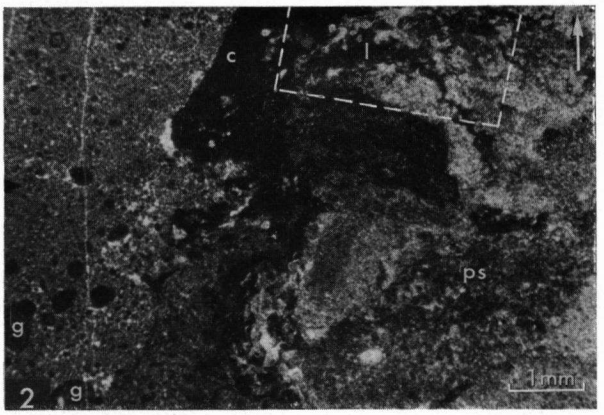
c
l
ps
g
g
1mm

2

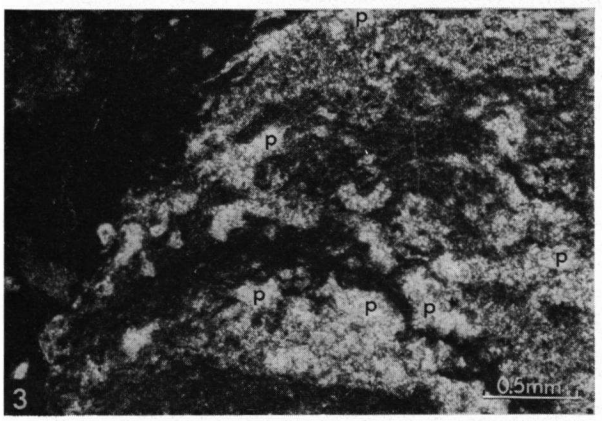
p
p
p
p
p
p
p
0.5mm

3

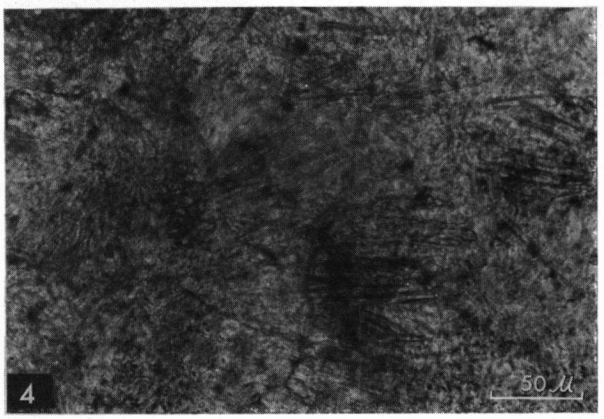
50 μ

4

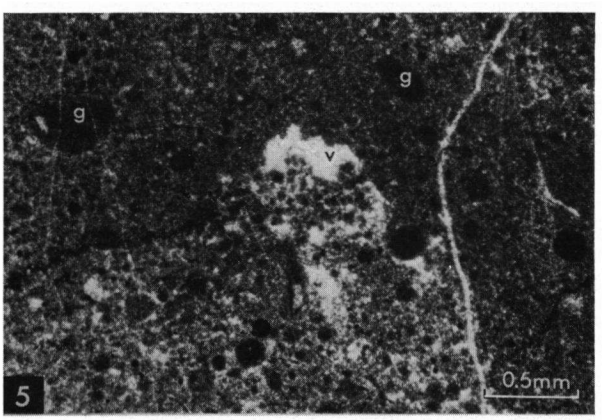
g
g
v
0.5mm

5

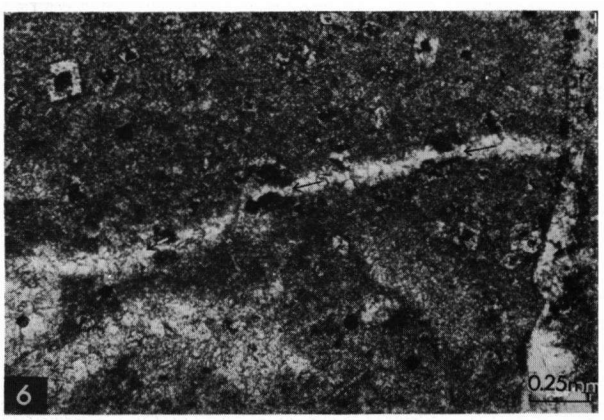
0.25mm

6

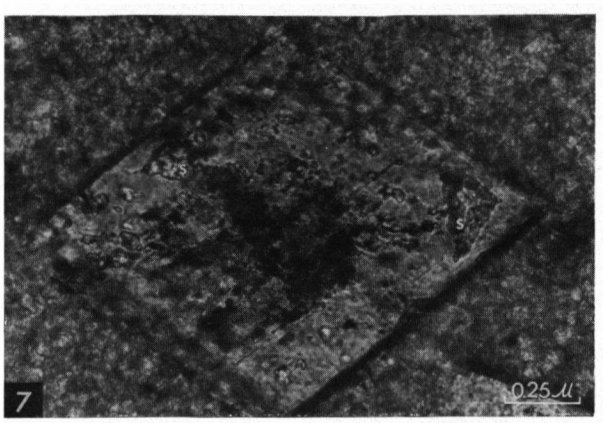
s
s
0.25 μ

7

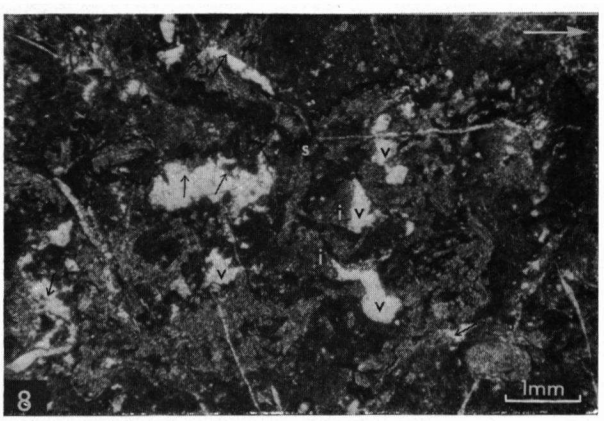
s
v
i
v
i
v
v
1mm

8

PLATE XI

Fig. 1. Dolo-wackestone with crinoid fragments, bryozoans and brachiopods. The micrite has been dolomitized completely. The bioclasts show only local dolomitization. The large crinoid fragment in the center shows algal coating and micritization. LSW 102.

Fig. 2. Detail of the central crinoid fragment of Fig. 1. Clusters of dolomite rhombs developed preferably in places of heavy micritization (arrows).

Fig. 3. Brachiopod with internal sediment which has not been dolomitized or only slightly, perhaps because of its pseudostromatic nature (see the sections "internal sediment" and "dolomite replacing micrite and pseudospar"). Algal micrite patches (a) outside the shell also resisted dolomitization. LSW 102.

Fig. 4. Brachiopod with completely dolomitized internal sediment. b-bryozoan fragment; s-spherulite. LSW 102.

Fig. 5. Detail of Fig. 4 showing preferred dolomitization of pore-filling calcite with micrite inclusions (arrows). LSW 102.

Fig. 6. Indiscriminate solution enlarged a pore network of constructed voids and crumbly fractures. Bryozoans (b) adjacent to the voids are partly dissolved. Micrite patches "float" in the sparry calcite. Where the solution was not sufficient to dissolve the algal-bound micrite completely, neomorphic calcite was created (lighter colored patches). The latter has been dolomitized selectively with respect to the unleached micrite. LSW 103.

Fig. 7. Detail of the uppermost bryozoan of Fig. 5. Part of its outer wall has been dissolved. The bryozoan is surrounded by clear pore-filing calcite and patches of selectively dolomitized neomorphic calcite.

Fig. 8. Pore-fill algal mold, enlarged by indiscriminate solution; dashed line indicates original outline of the algal fragment. i-floor of internal sediment contrasting with the surrounding algal-bound micrite. LSW 103.

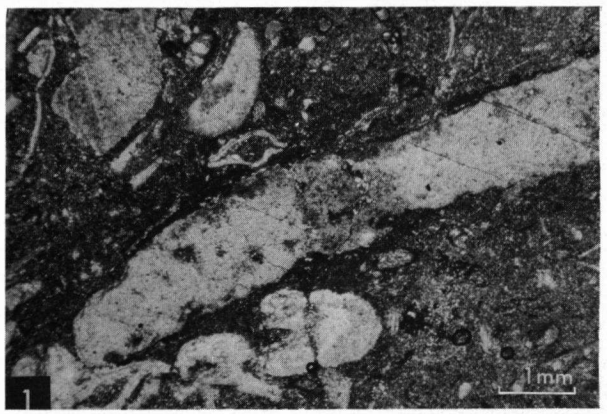
1
1mm

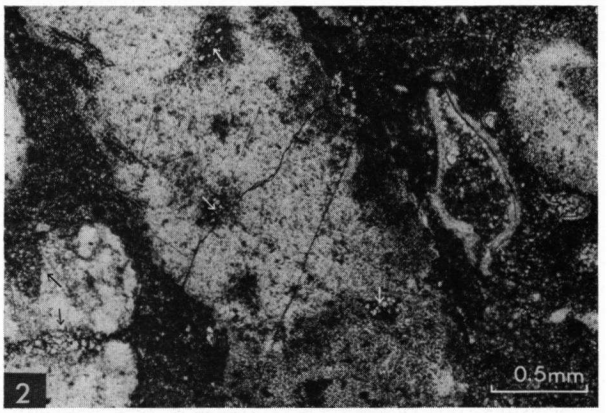
2
0.5mm

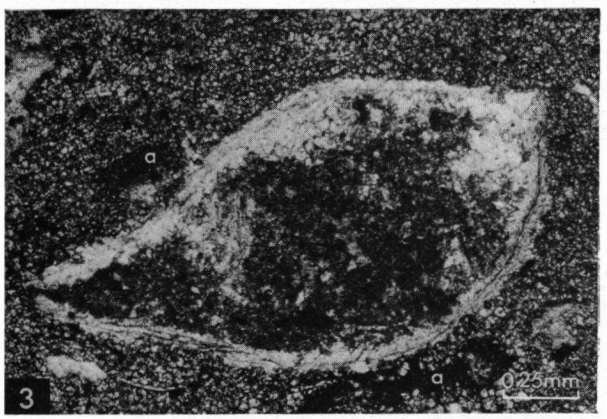
a
a
3
0.25mm


s
b
4
0.25mm

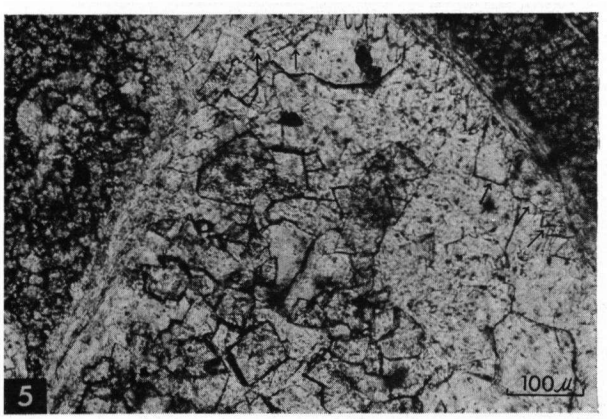
5
100μ

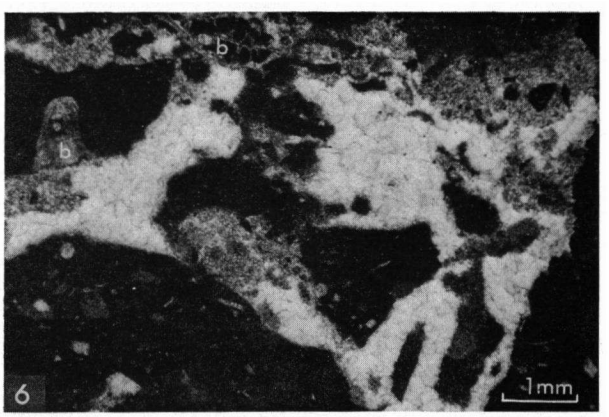
b
b
6
1mm

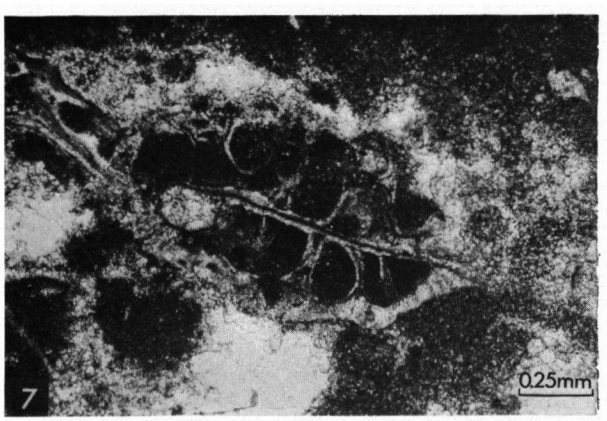
7
0.25mm

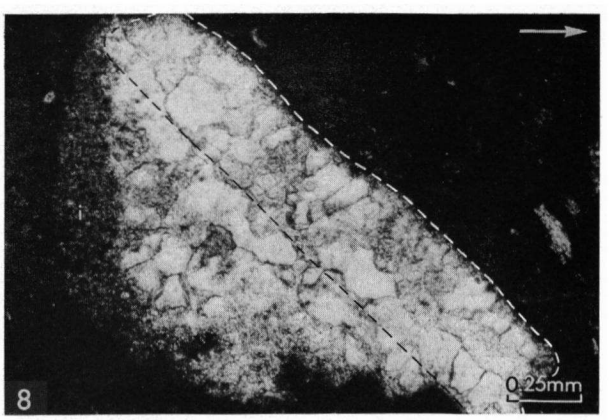
8
0.25mm

PLATE XII

Fig. 1. Algal-bound lime mudstone with pore-fill fossil molds and small constructed voids (black), both with floors of internal sediment (i). Tightly bound pseudostromatic parts are white in this figure. Two sets of parallel sharp-edged fractures are present (N-S and E-W). cr-crumbly fractures; v-solution void. LSW 104. Negative print of thin section.

Fig. 2. Local algal mat lamination. Within the dark pseudostroma (upper part of the figure) a lamination (1) is visible due to local calcification of algal tubes. LSW 105.

Figs. 3. and 4. Transverse section through the shell of a brachiopod. The rhombohedral pattern of the prisms of the microstructure of the upper valve continues into the bladed overgrowth. A microstructure of perpendicularly oriented large prisms is suggested. Inclusions of a light internal algal coating in the overgrowth help in tracing the original outline of the valve. If such an internal algal coating is not present it is sometimes impossible to distinguish the valve from the overgrowth. The brachiopod is surrounded by pseudostromatic micrite with a constructed void (v). Despite the external algal coating on the brachiopod valve the pore-filling calcite of the void is partially syntaxial with the microstructure. LSW 107.

Fig. 4. See Fig. 3. × nicols.

Fig. 5. Detail of Fig. 3 (part). Internal sediment of the brachiopod. The upper part of the figure shows consumption of the internal sediment by the pore-filling calcite. Only indigestible inclusions are visible in the big calcite crystals. The lower part of the figure shows neomorphism of the micritic internal sediment comparable to neomorphism of algal-bound micrite. The initial high porosity of the mechanically deposited internal sediment was not reduced by compaction due to the absence of an overburden. Inclusion of the micrite in pore-filling calcite crystals caused neomorphism. b-brachiopod valve. Phase-contrast.

Fig. 6. Detail of Fig. 5. Local dolomite rhombs in the neomorphic internal sediment. The sediment surrounding the brachiopod is pseudostromatic (see Figs. 3 and 4). The original composition of the internal sediment of the brachiopod, although mechanically deposited but most likely derived from the surrounding sediment, consequently will have been a high Mg calcite. During recrystallization into stable low Mg calcite initial dolomite rhombs (white arrows) developed locally by liberation of Mg-ions. Further growth of the rhombs (black arrows) took place by additional supply of magnesium from the Mg-enriched interstitial water of this dolomitic sample (see the section "hypotheses on the dolomitization process"). Phase-contrast.

Fig. 7. Centripetal replacement of dolomite rhombs by calcite caused relict dolomite anhedra. Zones of impurities originally lining the dolomite rhombs, by partial regeneration of the micrite mosaic now show as irregular "reaction" rims. A wide sharp-edged fracture transects the dolomite crystals. A smaller one tends to break around the dolomite crystals. LSW 109. Phase-contrast.

Fig. 8. Sharp-edged fracture with neomorphic micrite (1) transected by sharp-edged fracture (2) with pseudospar (see the section "pseudospar in relation to fractures"). The offset part of fracture (1) is visible on the left side of fracture (2). White patches in the dark micrite are pore-fill fossil molds. v-constructed void with floor of internal sediment, transected by fracture (2). LSW 111.

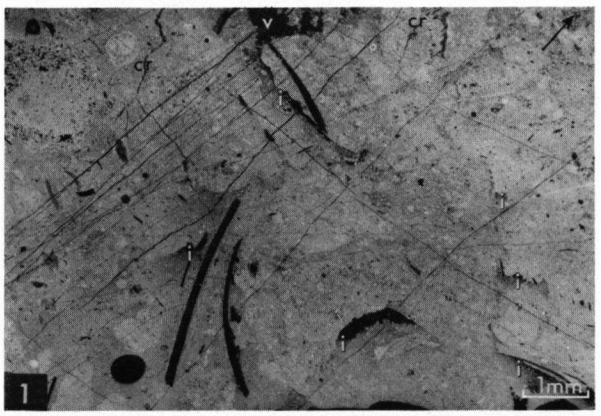
v
cr
cr
1
1
1
1
1
1mm
1

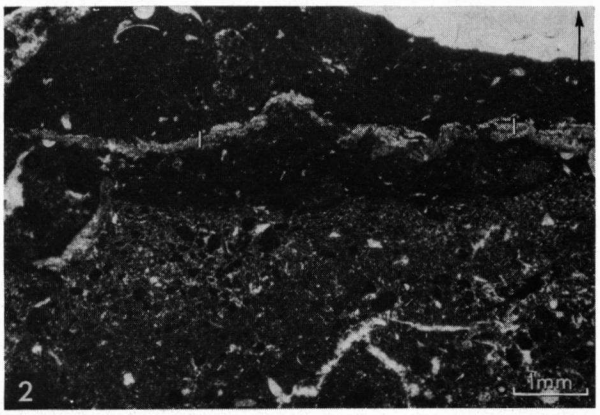
1
1
1mm
2

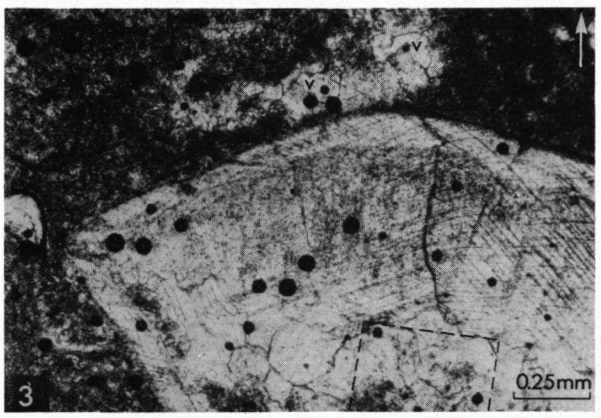
v
v
0.25mm
3

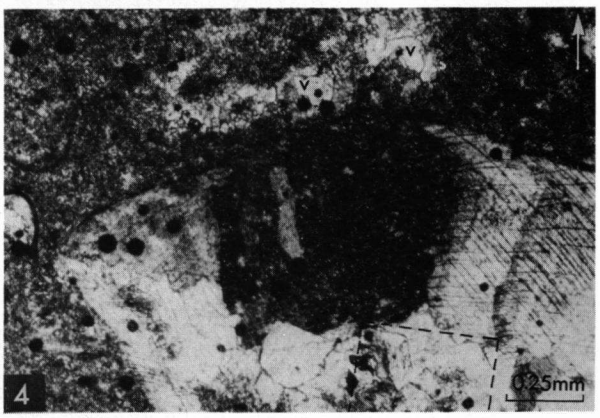
v
v
0.25mm
4

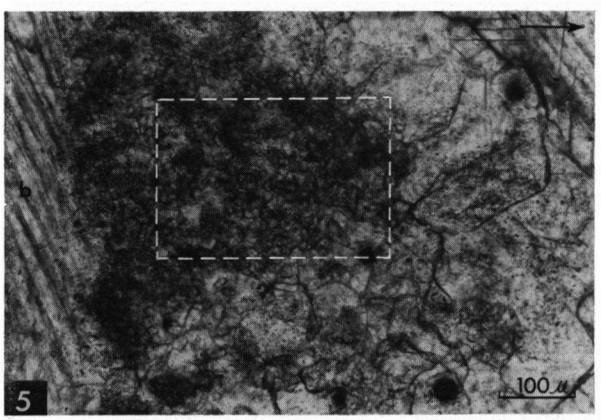
b
100 μ
5

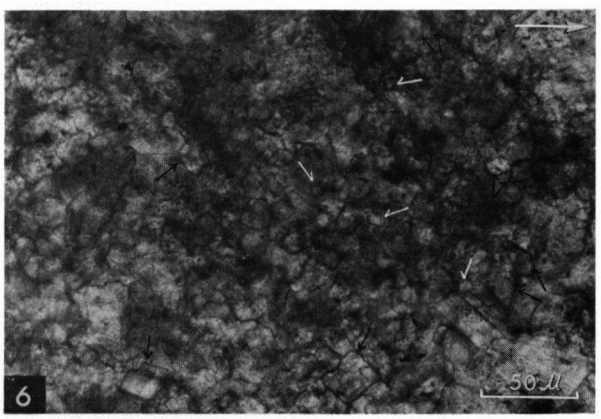
50 μ
6

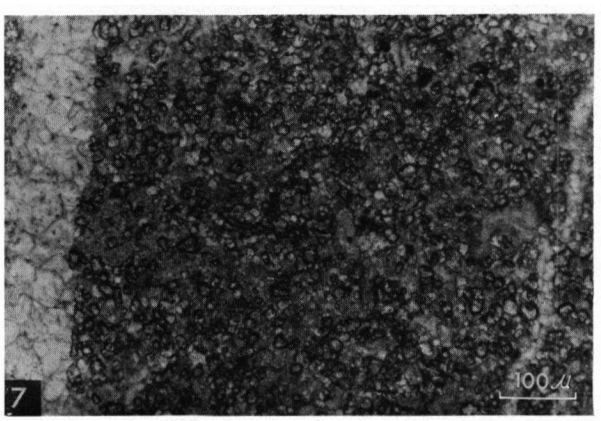
100 μ
7


v
1
2
1
1mm
8

PLATE XIII

Fig. 1. Solution stringers in mechanically deposited lime wackestone. Crinoid fragment in the center. LSW 113.

Fig. 2 and 3. Detail of Fig. 1 showing the heavy micritized crinoid stemfragment. The original network of the skeleton has been preserved locally as follows: the original network of the skeleton was micritized and the pores in it filled with clear calcite (arrows). Elsewhere the network was partially micritized and the pores were filled with both algal micrite and calcite. As a result the network of the original skeleton has been obliterated and a calcite crystal with micrite inclusions developed. Deep black: iron mineralizations. At the location of the central channel, filled syntaxially with clear calcite, a microscopically small fracture is visible at the brecciated zone in the center of the channel. The fracture caused slight deviation of the right part of the crinoid fragment indicated by slightly different position of extinction under crossed nicols. Fig. 2 // nicols.

Fig. 3. See Fig. 2. × nicols.

Fig. 4. Compaction before pore-filling with calcite generation 1b is indicated by the crushed brachiopod valve since the internal void was filled after crushing. The pseudostromatic micrite above the brachiopod lacks any sign of compaction. Constructed voids (v) in it remained open and were filled with pore-filling calcite 1b. u-*Ungdarella* sp., cross sections; d-*Dvinella* sp., cross sections; s-stylolite. LSW 115.

Fig. 5. Sharp-edged fracture transecting a dolomite crystal. Partial calcitization of the latter has partly regenerated the original micrite mosaic. Dispersed in the micrite are other partially calcitized dolomite crystals. e-echinoderm fragment with a completely dolomitized algal coating. Calcitization of the dolomite partly regenerated this algal coating. LSW 117. Phase-contrast.

Fig. 6. Detail of another dolomite crystal of LSW 117, transected by a sharp-edged fracture (f). s-silicified patches within the partially calcitized dolomite crystal; m-regenerated micrite mosaic. Phase-contrast.

Fig. 7. Euhedral overgrowths on transected dolomite crystals into the void of a sharp-edged fracture. Both the euhedral overgrowths and the transected dolomite crystals have been partially calcitized. In the transected crystals this is visible as the regenerated micrite mosaic and the resulting obliteration of the outlines of the crystals. In the euhedral overgrowths calcitization can only be demonstrated by a color photo of the slide colored in Alizarin Red-S.

Fig. 8. Two pseudostromatic bodies (ps) with a solution stringer (s) in between. Compaction started before pore filling with calcite generation 1b. The mold of *Anthracoporella* sp. (a) was compressed before its internal void was filled. p-algal plates encrusting mechanically deposited debris; br-bryozoan; d-*Dvinella comata* Chvorova, 1949.

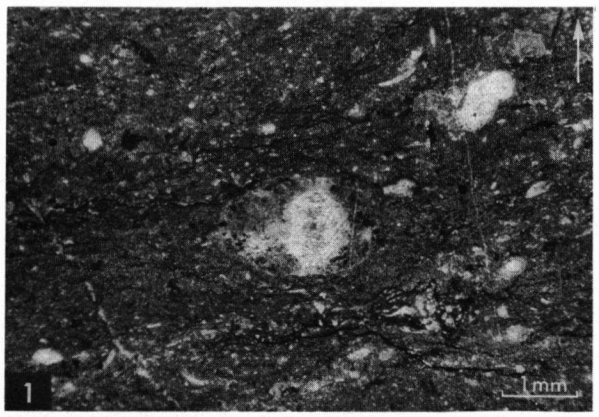
1
1mm

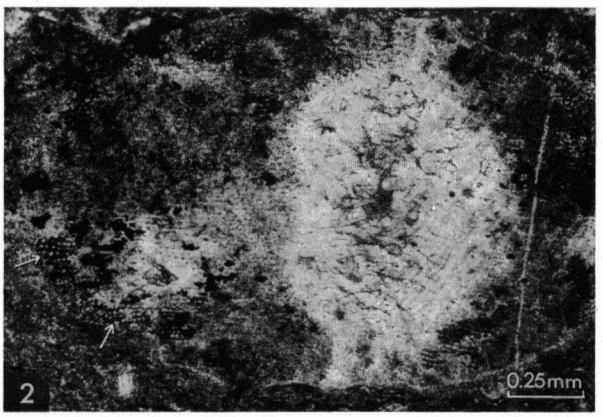
2
0.25mm

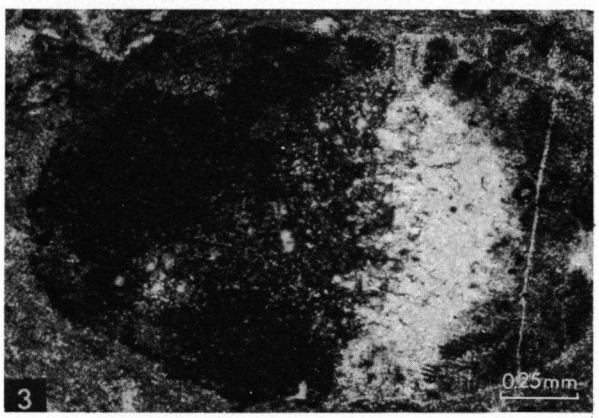
3
0.25mm

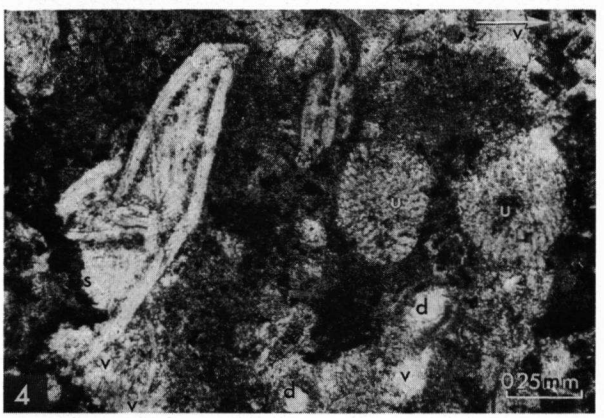
4
v
u
u
s
d
v
v
d
v
0.25mm

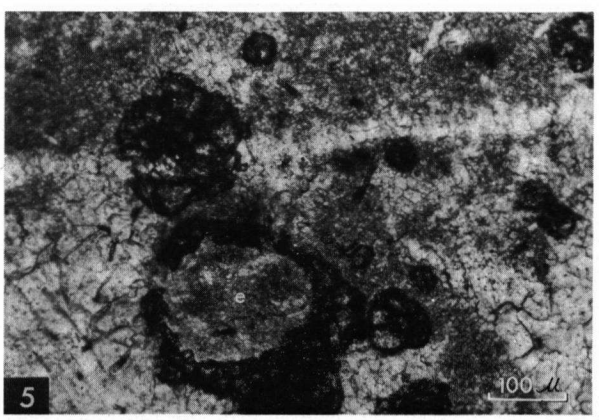
5
e
100 µ

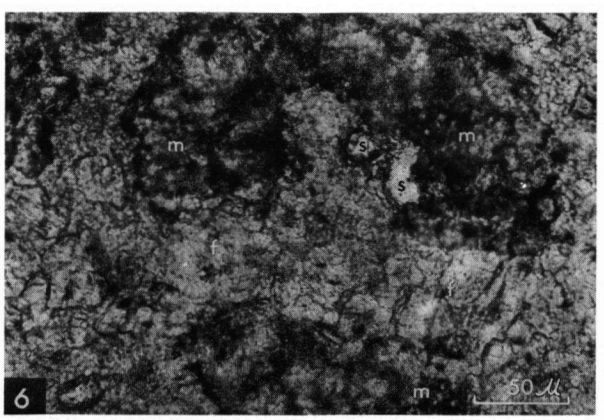
6
m
s
m
s
f
f
m
50 µ

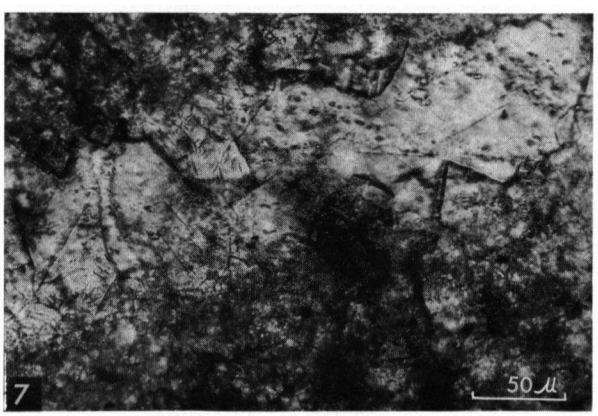
7
50 µ


8
ps
s
ps
d
br
p
p
1mm

PLATE XIV

Fig. 1. Erect specimen of *Archaeolithophyllum* sp. (a) broken by compaction pressure. m-algal molds of unidentifiable micritized and aggraded neomorphic Algae; an-flat lying *Anthracoporella* sp. surrounded by an algal debris packstone which originated by compaction of a wackestone; solution stringers indicate voidless solution of the micrite; s-solution stringers in mechanically deposited wackestone; p-pseudostromatic body lacking compaction phenomena; t-encrusting calcareous algal tubes. LSW 122.

Fig. 2. *Anthracoporella* sp. (a) with thick pseudostromatic algal coating lacking compaction and contrasting with the overlying mechanically deposited original wackestone compressed into a packstone. s-solution stringers; v-constructed void. LSW 122.

Fig. 3. Wedge of mechanically deposited micrite with solution stringers, intercalated in an algal-bound pseudostromatic lime wackestone with pore-fill fossil molds. LSW 123.

Fig. 4. Growth in situ of calcareous algal tubes (t) in a dark algal coating contrary to gravity over a grumous, pelletous pseudostromatic body with constructed voids (v) and a pore-fill fossil mold (m). g-algal grain. On top of the pseudostromatic body pseudostromatic micrite again formed. LSW 126.

Fig. 5. Algal grain, probably derived from a pseudostromatic body or from calcification of a colony of unicellular Algae. LSW 128.

Fig. 6. Detail of Fig. 5 showing algal pellets, neomorphic micrite and pseudospar within the algal grain.

Fig. 7. Pore-filling calcite of a gastropod mold integrated with the pore-filling calcite of an indiscriminate solution void (v). LSW 129.

Fig. 8. Pore network of indiscriminate solution voids. The algal-bound packstone with bryozoan fragments, which are partly dissolved when adjacent to a solution void, is black in this figure. Leached, incompletely dissolved algal-bound micrite patches, recrystallized during impregnation with calcium carbonate-rich solutions (see the section "neomorphic calcite creating solution"). e-echinoderm fragment; s-stylolite. LSW 129.

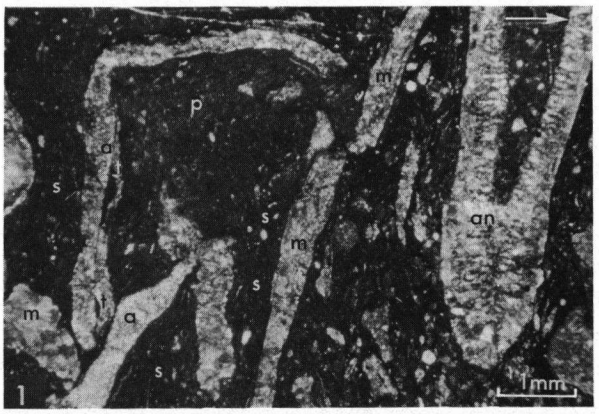
p
m
s
a
s
m
an
s
m
a
s
1mm
1

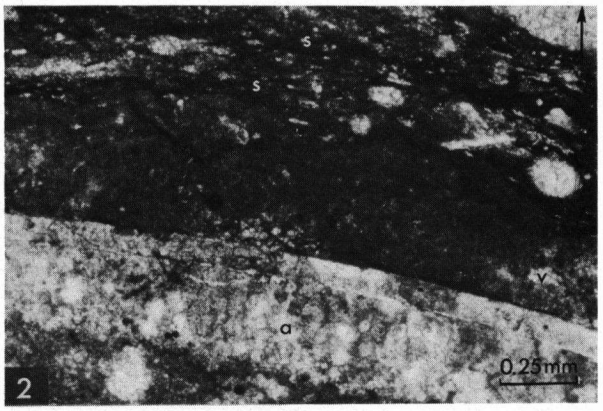
s
s
v
a
0.25mm
2

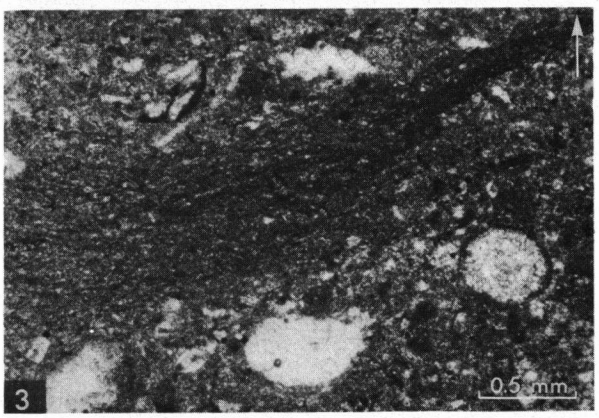
0.5 mm
3

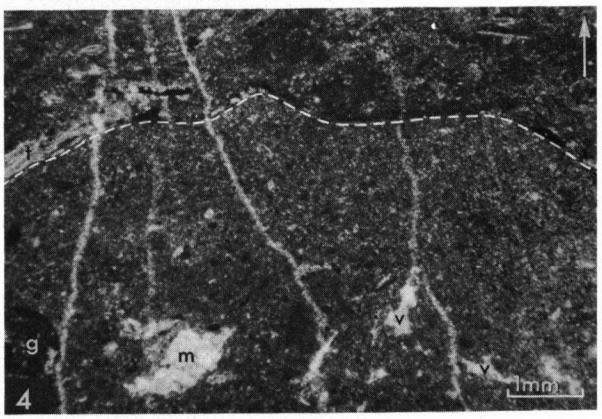
g
m
v
v
1mm
4

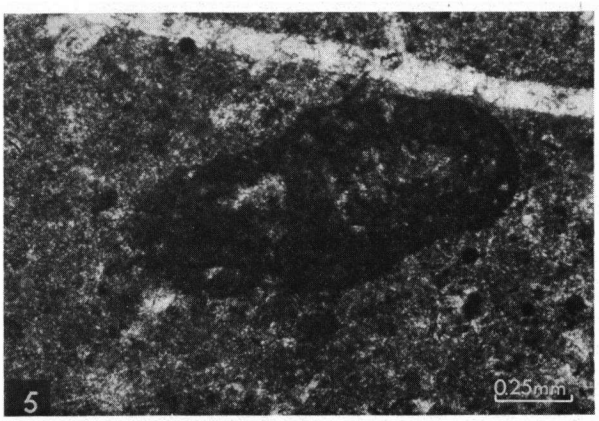
0.25mm
5

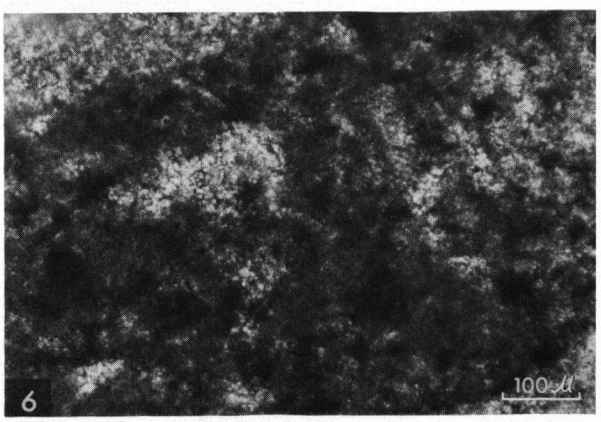
100 µ
6

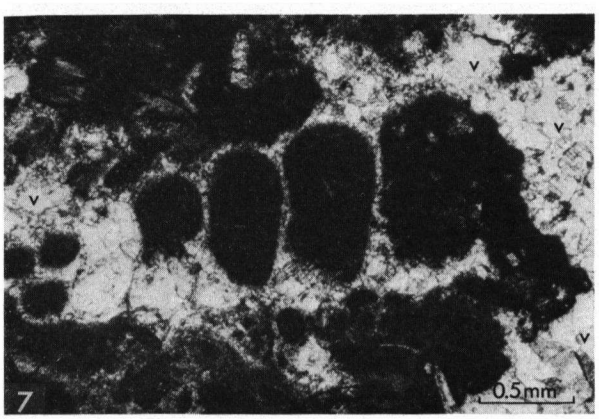
v
v
v
v
v
0.5mm
7

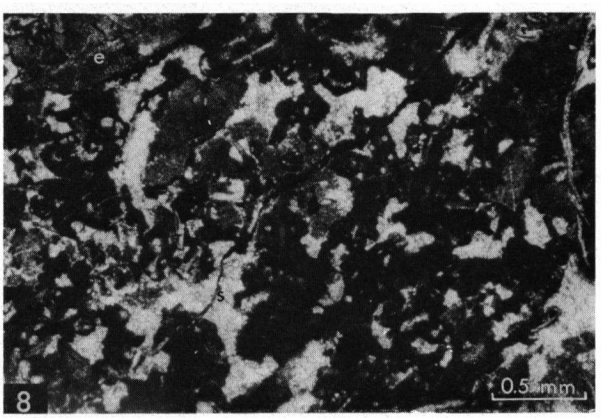
e
s
0.5 mm
8

PLATE XV

Fig. 1. Solution void (v) in internal sediment of a pore-fill mold of *Anthracoporella* sp. The pore-fill mold and the solution void were filled with the same generation of pore-filling calcite 1b. m-pore-fill fossil mold transected by a sharp-edged fracture containing pore-filling calcite with micrite inclusions and pseudospar. br-bryozoan. LSW 133.

Fig. 2. Pore network of pore-fill molds connected by crumbly fractures (cr). The pore-fill molds were enlarged by indiscriminate solution. LSW 140.

Fig. 3. Integrated mosaics of pore-filling calcite in a crumbly fracture (cr) and a pore-fill fossil mold (m). LSW 140.

Fig. 4. Algal-bound *Ungdarella* (u) and *Dvinella* (d) lime packstone. The interstices are locally lined with pore-filling calcite 1a (arrows). After crumbly fracturing the interstices have been enlarged by solution, indiscriminately attacking the fibrous crust 1a, bioclasts and the micrite matrix. ps-pseudostromata. LSW 142.

Fig. 5. Crumbly fracture (cr) transecting fibrous crust 1a. d-*Dvinella*, cross section, with a neomorphic, partly dissolved fibrous crust 1a. Interstice filled with pore-filling calcite 1b. LSW 142. Phase-contrast.

Fig. 6. Intergrowth of *Dvinella comata* Chvorova, 1949. Interstices are filled with pelletous pseudostromata. Crumbly fractures (cr) transect and offset some specimens of *Dvinella*; together with constructed voids, enlarged by indiscriminate solution, they form a pore network. f-sharp-edged fractures. LSW 148.

Fig. 7. Intraclast lime packstone. The intraclasts are angular fragments of an early consolidated algal-bound *Ungdarella* and *Dvinella* lime packstone. LSW 150.

Fig. 8. Detail of Fig. 7. d-*Dvinella comata* Chvorova, 1949; u-*Ungdarella* sp.

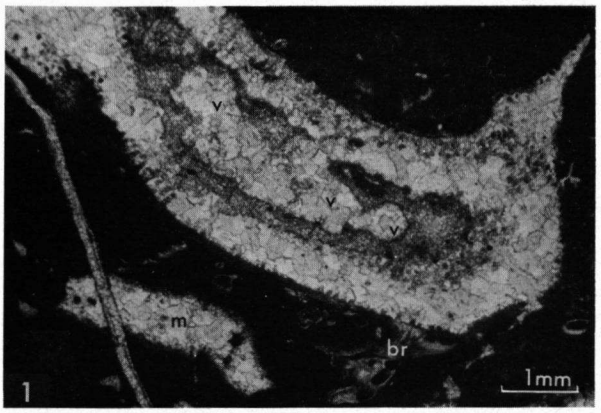
v
v
v
m
br
1mm
1

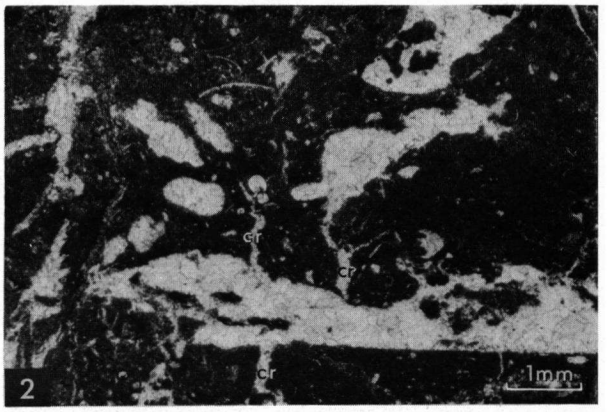
cr
cr
cr
1mm
2

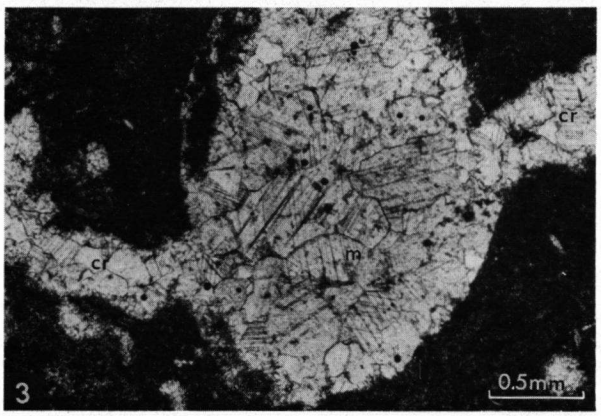
cr
cr
m
0.5mm
3

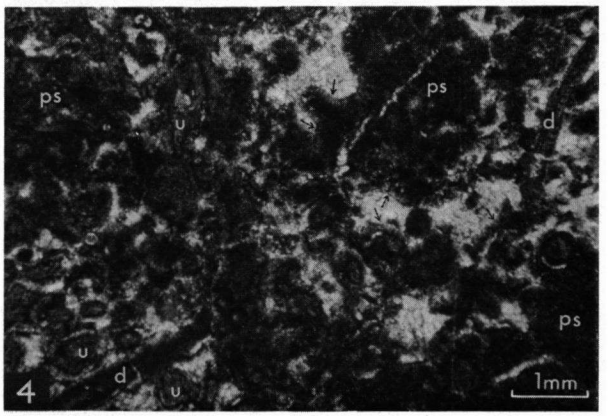
ps
u
ps
d
ps
u
d
u
1mm
4

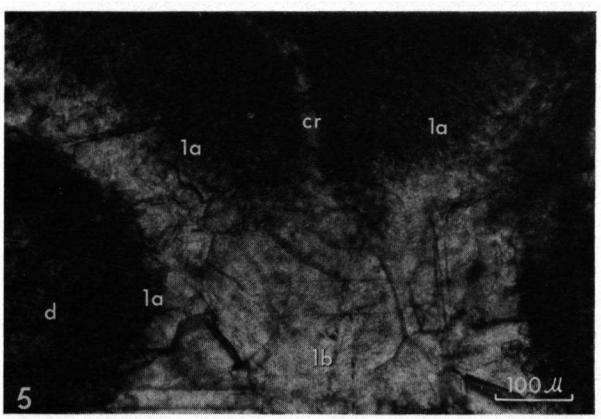
cr
1a
1a
d
1a
1b
100 μ
5

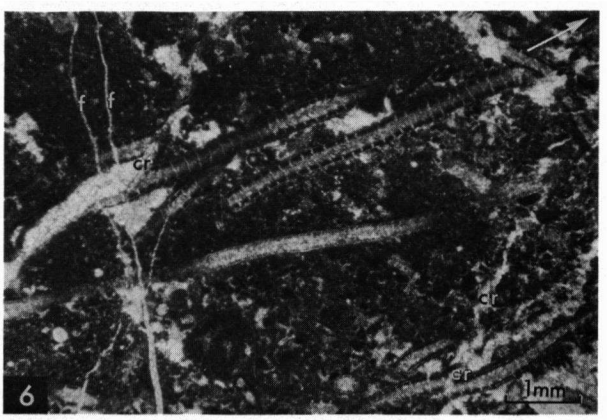
f
f
cr
cr
cr
1mm
6

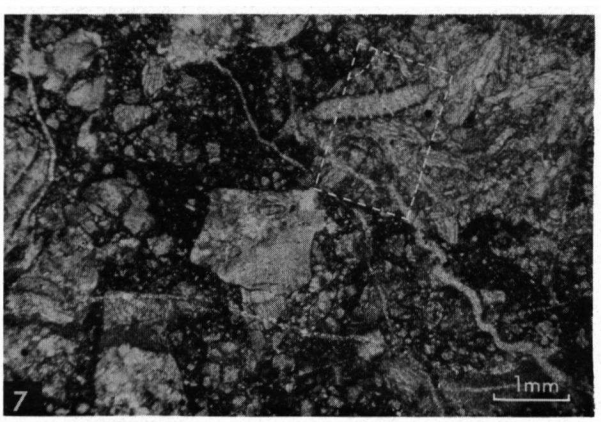
1mm
7

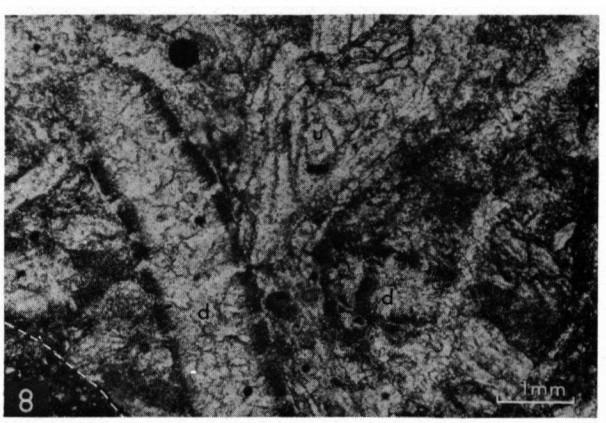
u
d
d
1mm
8

PLATE XVI

Fig. 1. Micritized relicts of a dasycladacean Alga embedded in neomorphic pseudostromatic micrite and pseudospar. Part of the micritized Alga is also neomorphic and lacks relicts of the algal structure, probably indicating that neomorphism was related to solution. The lower part of the figure shows a mechanically deposited wackestone with solution stringers resulting from compaction. LSW 151.

Fig. 2. Pseudostromatic body with pore-fill fossil molds (black) contrasting with surrounding mechanically deposited micrite. LSW 152. Negative print of thin section.

Fig. 3. Lime packstone formed by prolific delivery of bioclasts in an environment of algal micrite precipitation. Algal binding was not sufficient to create a supporting framework. br-bryozoan fragment; u-*Ungdarella* sp. with algal coating and micritization; b-*Beedeina* sp.; t-trilobite fragments; s-smaller Foraminifera. LSW 153.

Fig. 4. Detail of Fig. 3 showing embayed contacts between the allochems. t-trilobite fragments; u-*Ungdarella* sp. Phase-contrast. LSW 154.

5. Algal-bound lime wackestone with pseudostromatic patches which are clearly neomorphic and patches which are not algal bound but show compaction as indicated by the presence of parallel solution stringers. LSW 155.

Fig. 6. Detail of a neomorphic pseudostromatic body of LSW 155. Algal pellets and tiny bioclasts are "floating" in pseudospar and neomorphic micrite. Phase-contrast.

Fig. 7. Pelecypod valve surrounded by algal pellets and transected by a crumbly fracture (cr). The prisms of the normal prismatic microstructural layer show only slight recrystallization at the transection. h-enigmatic hemispherical organism which penetrated into the valve of the pelecypod; e-echinoderm fragment. LSW 156. × nicols.

Fig. 8. Local pseudostromatic patch (ps) within algal-bound lime packstone. p-pelecypod valve encrusted by calcareous algal tubes embedded in a dark algal coating. The encrusting calcareous algal tubes seem to protect the valve against micritization, since where they are missing the valve has been micritized completely (m). LSW 156.

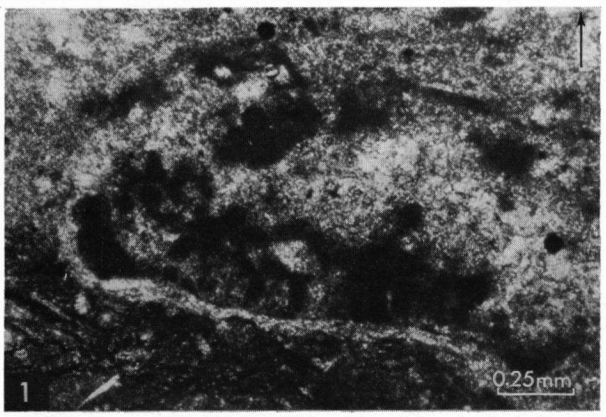
1
0.25mm

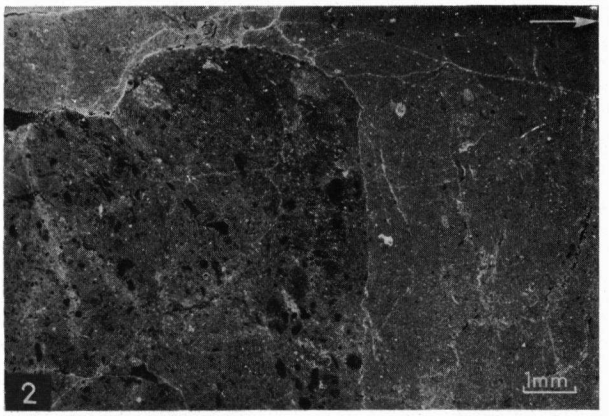
2
1mm

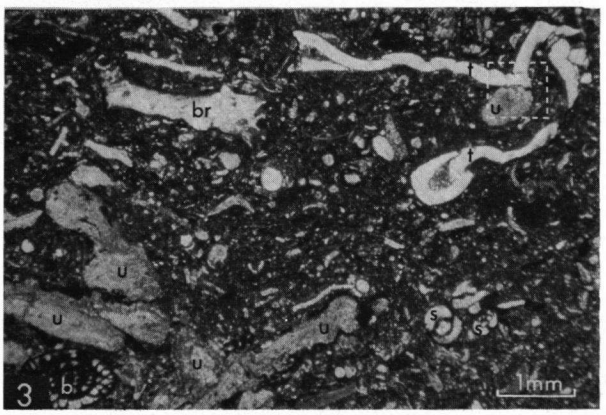
3
br
t
u
s
b
1mm

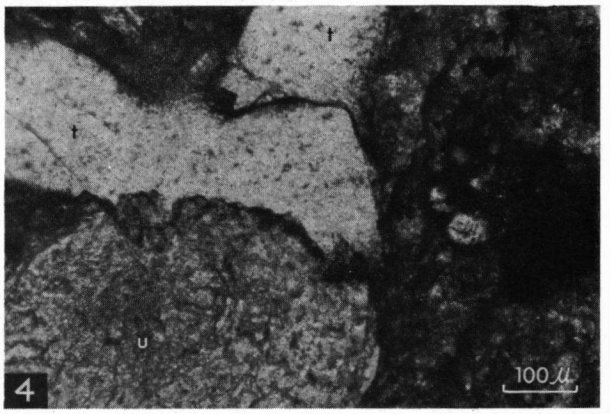
4
t
u
100 μ

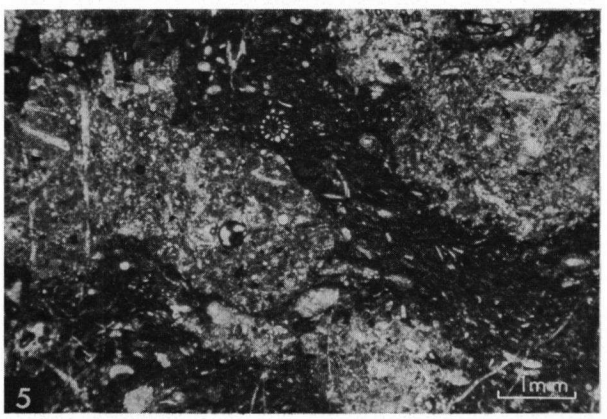
5
1mm

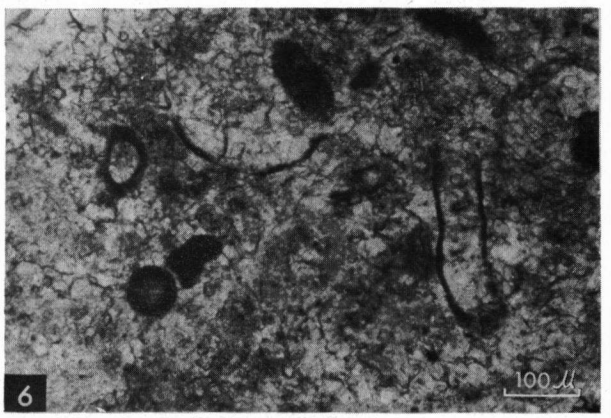
6
100 μ

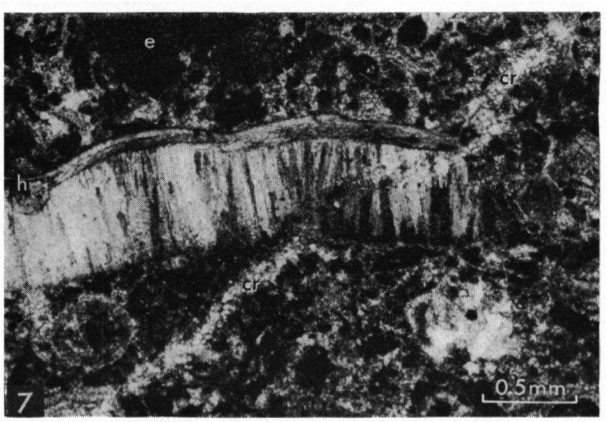
7
e
cr
h
cr
0.5mm

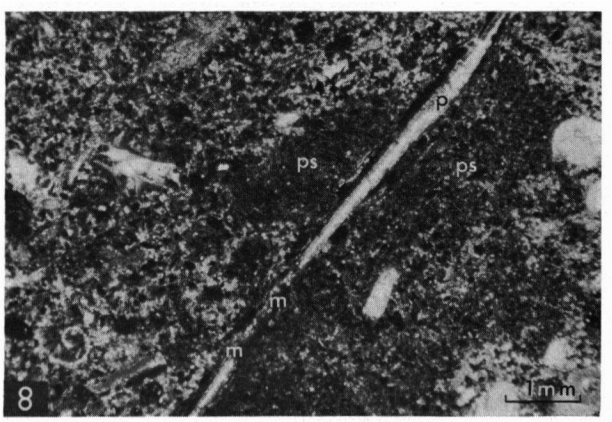
8
p
ps
ps
m
m
1mm

PLATE XVII

Fig. 1. Silicification (white patches) of the matrix of an algal-bound lime packstone. LSW 158. Phase-contrast.

Fig. 2. Algal-bound lime packstone with algal grains formed by micritization and algal coating of bioclasts. f-fusulinids, *Fusulina* sp., converted to algal grains; g-unidentifiable bioclast converted to algal grain. LSW 161.

Fig. 3. Detail of a fusulinid converted to an algal grain. Folded septa (arrows) are the only recognizable relicts of the original bioclast. The algal grain is surrounded by a matrix of neomorphic micrite and pseudospar. LSW 161.

Fig. 4. Algal-bound lime packstone with a dasycladacean Alga (d) converted into an algal grain and another dasycladacean Alga in the initial stage of transformation. The branches are partly filled with algal micrite; above the floor of internal sediment consisting of algal pellets and bioclasts, a grumous pelletous pseudostromatic body (ps) developed contrary to gravity (cf. the level of the internal sediment is indicated by a dashed line). LSW 164.

Fig. 5. e_1-micritized and recrystallized echinoderm fragment with algal coating; e_2-echinoderm fragment with micritized and subsequently recrystallized border (b). The original monocrystalline microstructure at the border has been lost. An adjacent pore when not filled with algal-bound micrite, is filled with calcite (s) syntaxial with the echinoderm fragment. LSW 168.

Fig. 6 and 7. Micritized and subsequently recrystallized (calcite cleavage) echinoderm fragment. The central channel has been filled with algal micrite. Neighboring pore spaces were filled with syntaxial overgrowths on the echinoderm fragment (Fig. 7). Locally the algal coating impeded the development of an overgrowth (arrows). Micrite matrix in pore spaces is neomorphic and grades to pseudospar. m-pore-fill mold with algal coating; br-fragment of a fenestrate bryozoan, micritized and algal-coated; f-fracture offsetting the echinoderm fragment. LSW 169. Fig. 6, // nicols.

Fig. 7. See Fig. 6. × nicols.

Fig. 8. Pore-fill molds (m) of codiacean Algae in situ, with thick algal coatings and relicts of undissolved micritized tubes along their walls. The surrounding sediment is pelletous pseudostromatic. LSW 174.

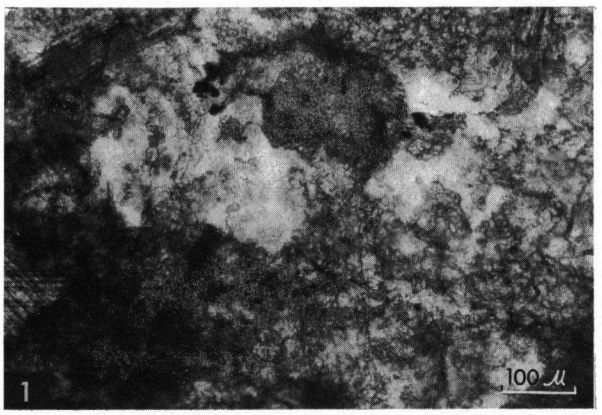
100 μ

1

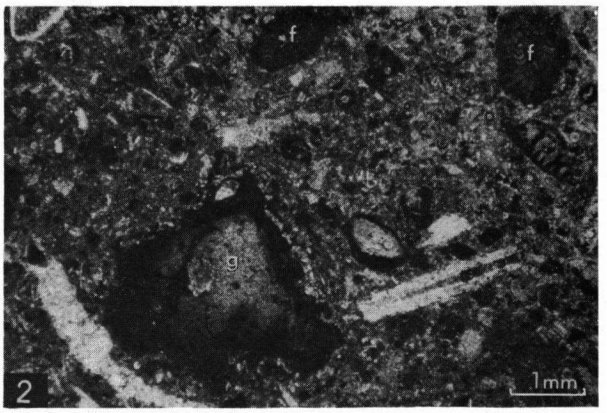
f
f
g
1mm

2


0.25mm

3

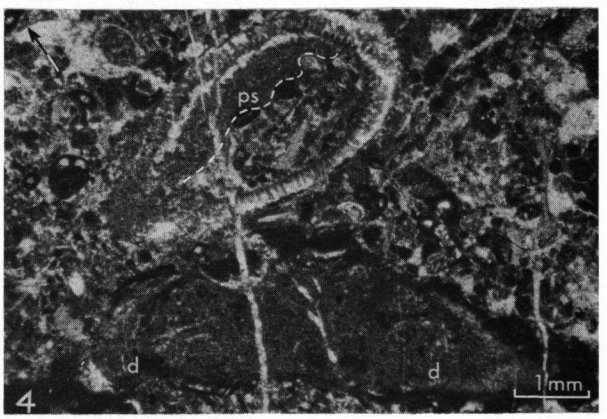
ps
d
d
1mm

4

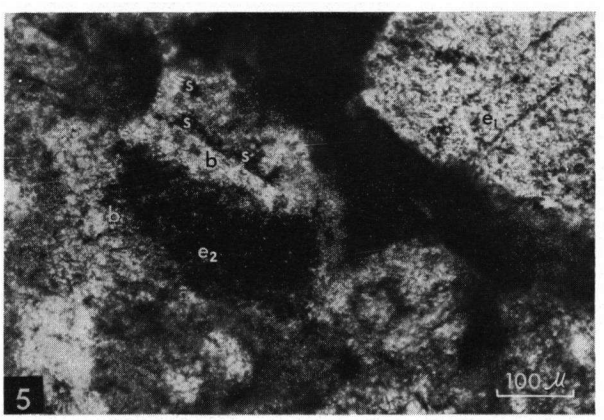
s
s
b
s
e1
b
e2
100 μ

5

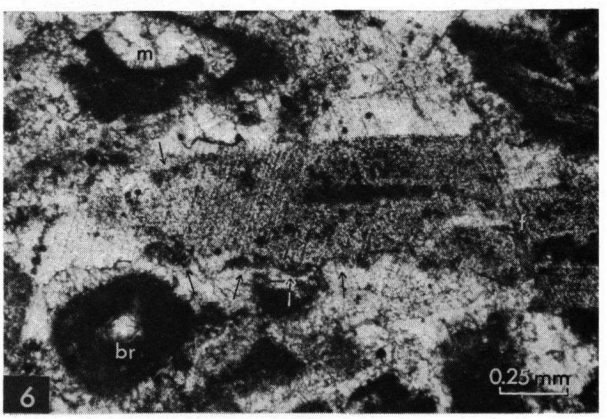
m
f
br
0.25mm

6

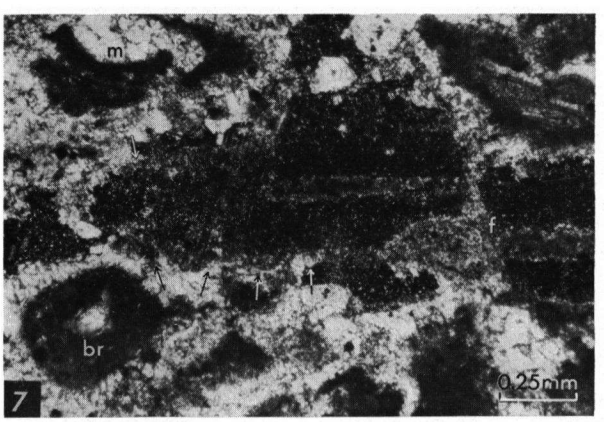
m
f
br
0.25mm

7

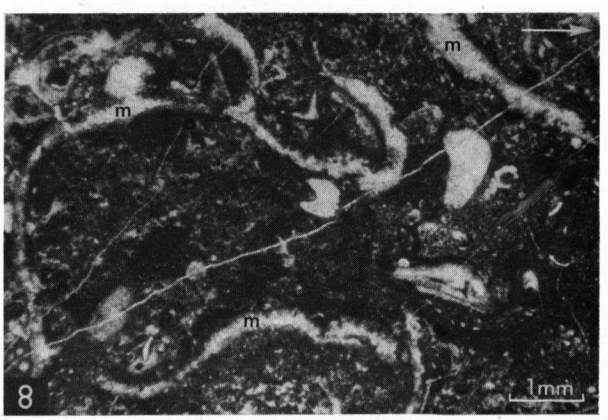
m
m
m
1mm

8

PLATE XVIII

Fig. 1. Bryozoan (br) in situ, surrounded by pseudostromatic micrite with pore-fill fossil molds. m-fossil mold filled with algal micrite. LSW 180.

Fig. 2. Algal-bound lime packstone with micritized and recrystallized (calcite cleavage) echinoderm fragments and micritized bryozoan fragments in exceedingly close packing. The little pore space left was filled with pseudostromatic micrite. A fusulinid, intermediate between *Eofusulina* and *Fusulina,* has a crushed outer whorl, but in general to few compaction phenomena are present for the packstone to be interpreted as being formed by compaction of a mechanically deposited wackestone. LSW 181.

Fig. 3. Algal-bound lime packstone with algal pellets and algal-coated neomorphic fossil molds (m). The matrix is neomorphic micrite and pseudospar. To the left two algal coated neomorphic fossil molds can barely be distinguished from the neomorphic matrix. q-quartz grain. LSW 182.

Figs. 4 and 5. Echinoid plate with tubercle surrounded by grumous pelletous pseudostromatic micrite with small constructed voids. The left edge of the echinoid plate borders a pore-fill fossil mold (m), filled by syntaxial overgrowth on the echinoid (Fig. 5). That this overgrowth is pore-filling and not displacing is demonstrated by the small rim (r) of pore-filling calcite crystals lining the void opposite the echinoid plate. It also demonstrates that pore-filling (cementation) by syntaxial overgrowth is much faster than pore-filling by crystal growth proceeding from the polynucleid borders of a void. v-small constructed void syntaxially filled by overgrowth on the echinoid plate. LSW 184. Fig. 4, // nicols. Fig. 5. See Fig. 4. × nicols.

Fig. 6. Micritized algal mold (m) in situ, surrounded by a pseudostromatic body (1). The algal-bound sediment formed a rich-relief overgrown contrary to gravity by a dark algal coating (c) which developed into a pseudostromatic body (2). Another algal coating contrary to gravity over pseudostromatic body (2) developed to the right (3). 4-pseudostromatic body overlain by mechanically deposited sediment with solution stringers; v-constructed voids; i-internal sediment. LSW 185.

Fig. 7. View to the left of micritized algal mold in Fig. 6 showing that at the top of pseudostromatic body (1) some sediment was deposited mechanically which was compressed by compaction contrary to gravity as shown by solution stringers (s). Pseudostromatic body (2) is also associated with an algal mold in situ, a primitive form of *Archaeolithophyllum* (a). Same symbols as in Fig. 6.

Fig. 8. Valve of a punctate brachiopod with algal coating, embedded in micrite formed by calcitization of dolomite (see the section "effect of calcitization of dolomite on dolomite content and texture"). LSW 185. Phase-contrast.

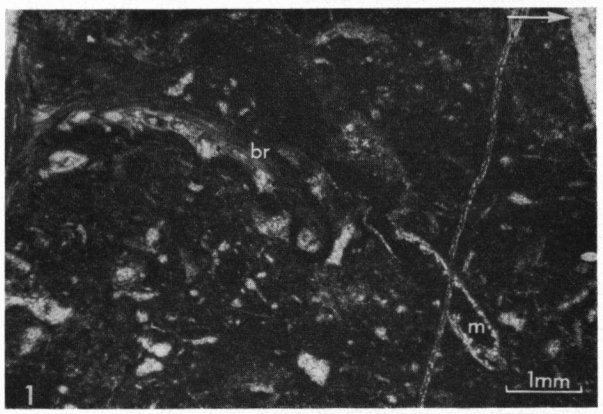
br
m
1mm
1

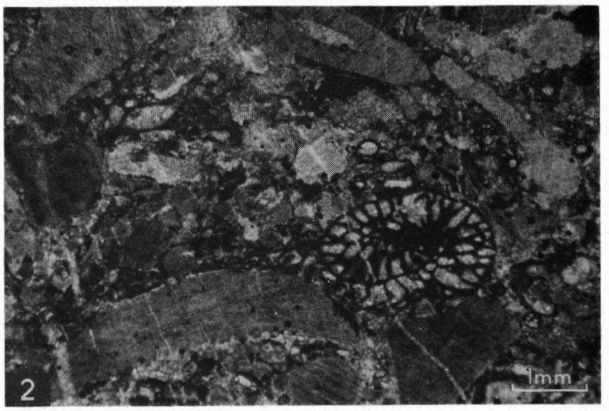
1mm
2

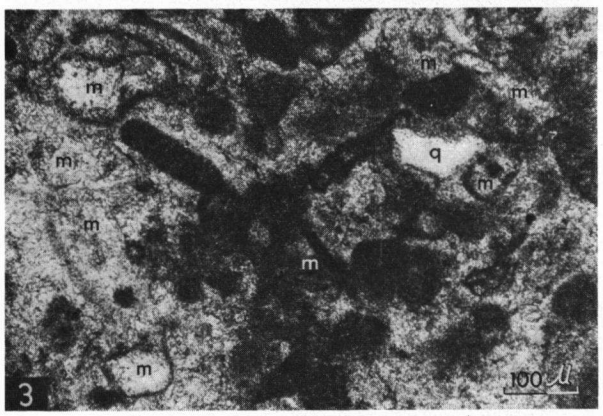
m
q
100 μ
3

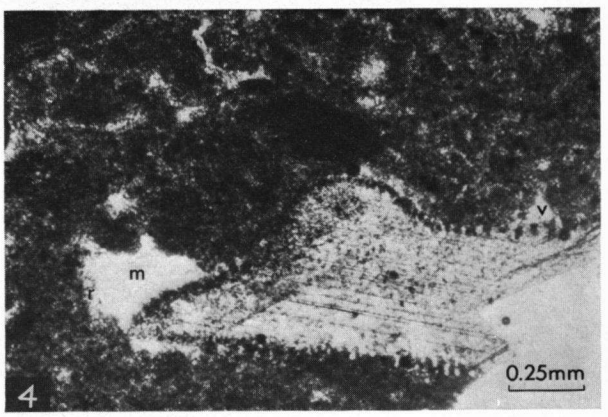
v
m
0.25mm
4

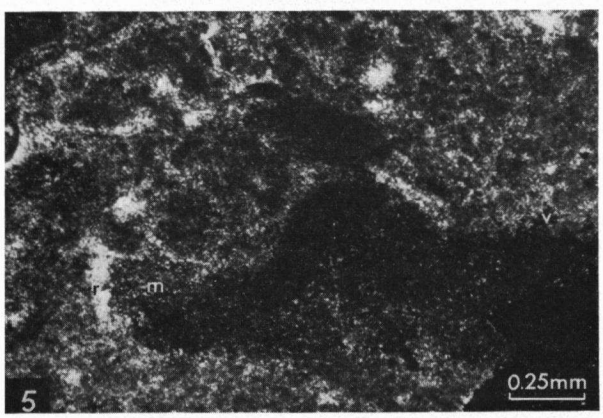
v
m
0.25mm
5

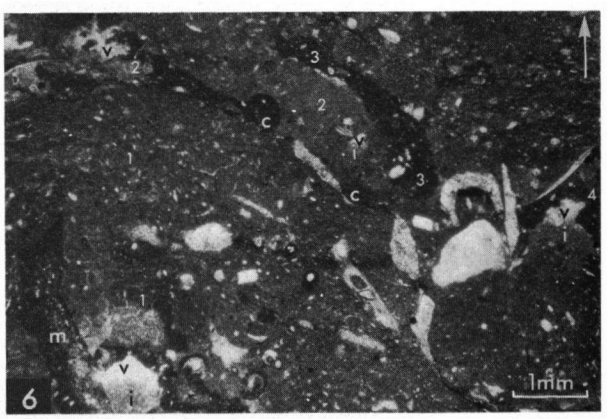
v
2
3
c
1
4
m
1mm
6

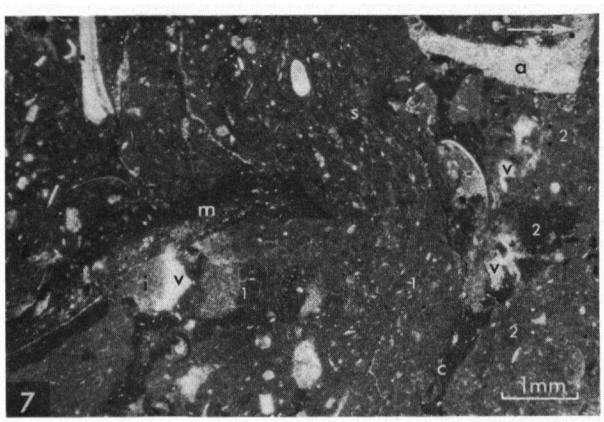
a
s
2
v
m
i
1
c
1mm
7

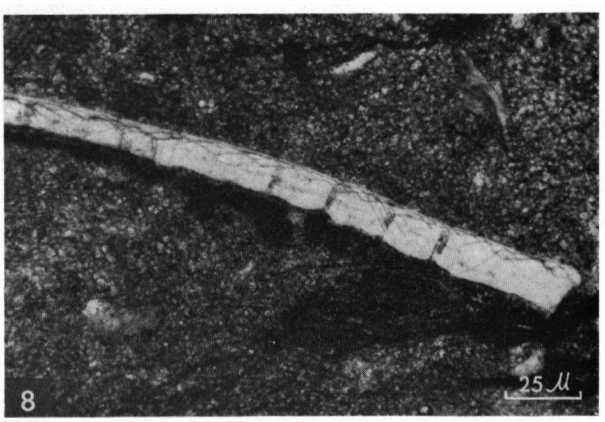
25 μ
8

PLATE XIX

Fig. 1. Solution voids (v), brecciated by crumbly fractures and enlarged later by solution; locally neomorphic calcite was formed. An algal micrite rim (r), lining the first phase solution voids, has been preserved only locally. The first phase of solution probably originated after an initial stage of crumbly fracturing or before any crumbly fracturing. If the latter applies then this is the only sample with evidence of solution before crumbly fracturing. LSW 190. Negative print of thin section.

Fig. 2. Detail of Fig. 1. Algal micrite rim (r) lining solution voids. cr-crumbly fractures; p-pseudospar formed by impregnation of the incompletely dissolved algal micrite rim by calcium carbonate-rich solutions; f-small sharp-edged fractures. LSW 190.

Fig. 3. Detail of the algal micrite rim (r) of Figs. 1 and 2. The algal micrite rim is neomorphic and grades to pseudospar. Phase-contrast.

Fig. 4. Detail of Fig. 3 showing micrite inclusions in the neomorphic micrite and pseudospar. Organic black streaks line the crystals. Phase-contrast.

Fig. 5. Algal-bound lime packstone with algal coated and micritized bryozoan fragments (br) and micritized fragments of the dasycladacean Alga *Epimastopora bodonensis* Rácz, 1965 (e), close to becoming algal grains (g). In the center a crinoid fragment (c) with a thin algal coating and algal boring channels (b), filled with algal micrite. The micrite matrix is neomorphic and grades via pseudospar to pore-filling calcite. LSW 191.

Fig. 6. Oncolite (o) around fragments of a dasycladacean Alga. Concentrically arranged calcareous algal tubes are embedded in the dark oncolitic coating. In places the oncolitic coating has dissolved or recrystallized (d). The dasycladacean fragments are pore-fill molds with micritized relicts of the algal structure. e-micritized fragments of *Epimastopora*. LSW 191.

Figs. 7 and 8. Micritized echinoderm fragment (e) with syntaxial overgrowth into an interstice between two oncolites (o). n-nucleus (pore-fill mold) of the left-hand oncolite; its oncolitic coating facing the interstice has been partly dissolved; m-patch of micrite enclosed in the overgrowth. LSW 191. // nicols.

Fig. 8. See Fig. 7. × nicols.

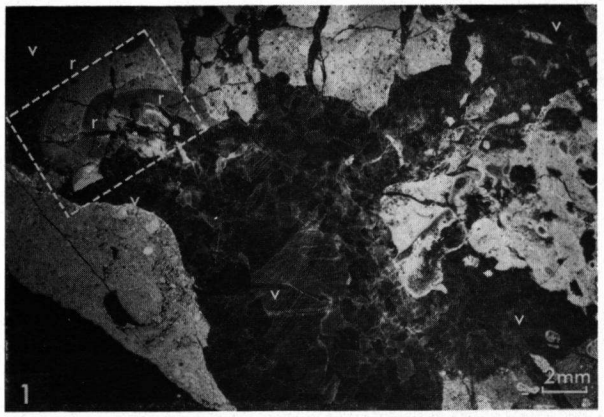
v
r
r
r
v
v
v
v
v
2mm
1

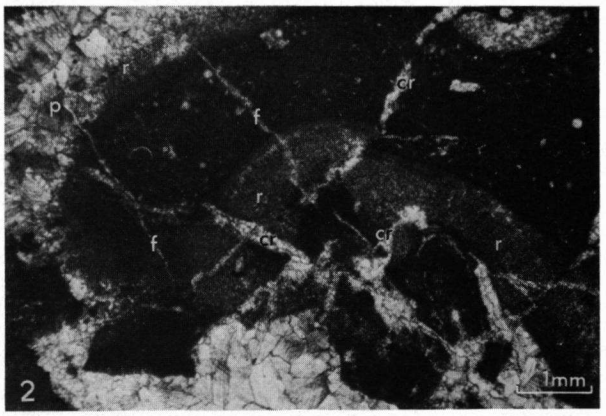
r
p
f
cr
r
f
cr
r
1mm
2

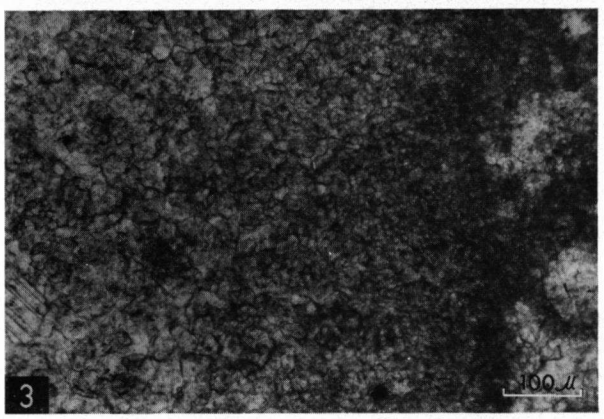
100 μ
3

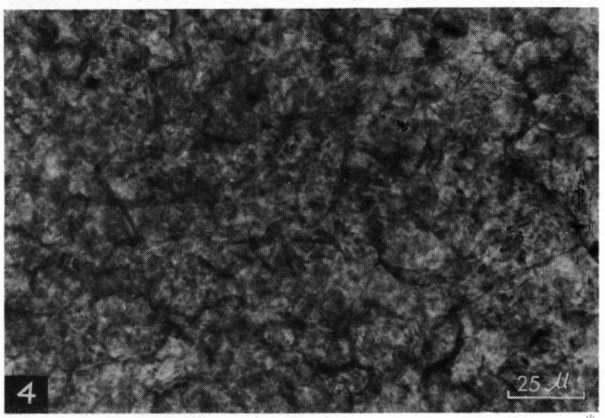
25 μ
4

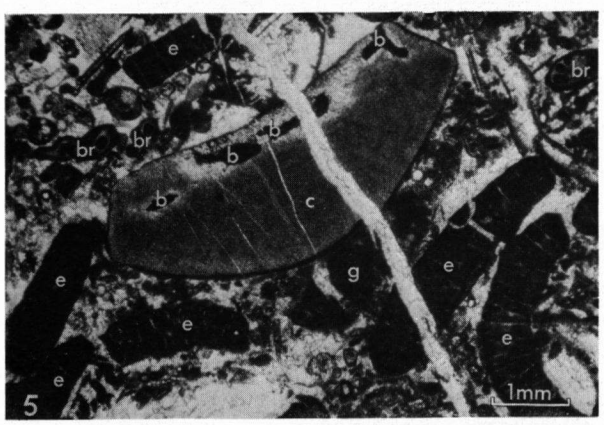
e
b
br
br
b
b
b
c
e
g
e
e
e
e
e
1mm
5

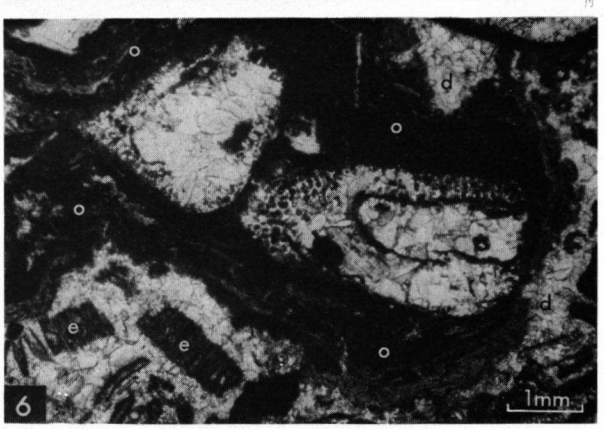
o
d
o
o
d
e
e
o
1mm
6

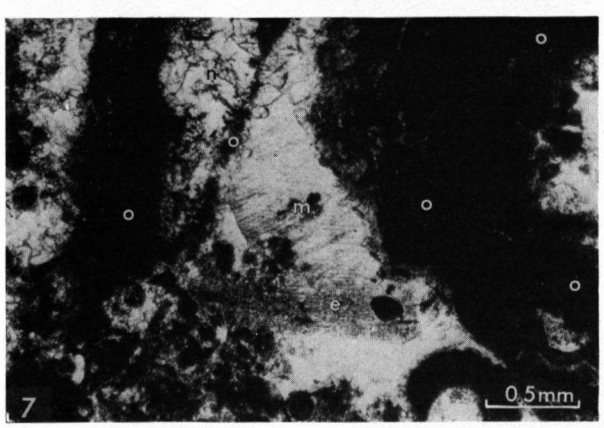
o
n
o
o
m
o
o
e
0,5mm
7

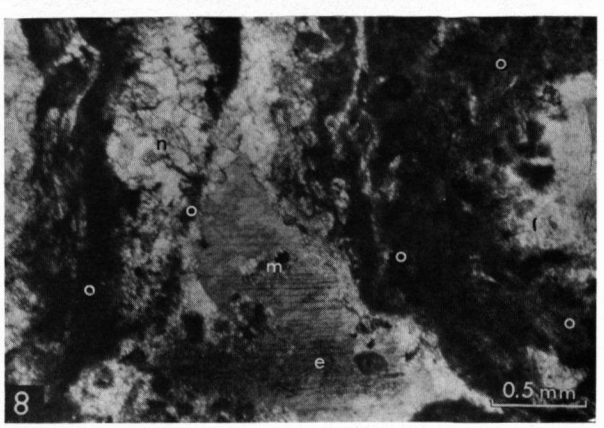
o
n
o
o
m
o
o
e
0.5 mm
8

PLATE XX

Figs. 1 and 2. Detail of Pl. XIX, Figs. 7 and 8, showing the patch of micrite (m) enclosed in the overgrowth. In Fig. 2 dolomite rhombs along the border of the micrite patch are clearly visible. LSW 191. Fig. 1, × nicols.
Fig. 2. See Fig. 1. Phase-contrast.
Fig. 3. Detail of Fig. 2. d-dolomite rhombs. Phase-contrast.
Fig. 4. Silicification in pseudospar. Slide has been etched by the acid admixture of Alizarin Red-S; as a result the silicified parts of the crystals show as islands. LSW 191. Phase-contrast.
Fig. 5. Silicification of a pore-filling calcite crystal following more or less the cleavage lines. LSW 191. Slightly etched thin section. Phase-contrast.
Fig. 6. Ultra-thin section of a dense pseudostromatic body showing an amoeboid mosaic of neomorphic micrite crystals with inclusions of original micrite, organic matter and clay-sized tubular quartz grains (see the section "neomorphic micrite"). LSW 1, southern flank of Lois Syncline West.
Fig. 7. More porous part of the pseudostromatic body of LSW 1 showing neomorphic micrite and pseudospar crystals, surrounded by pore-filling calcite crystals (p) with inclusions (focused on the inclusions in the neomorphic micrite and pseudospar crystals). The high relief of the neomorphic micrite and pseudospar is due to their resistance to etching by the acid admixture of Alizarin Red-S because of their relatively high proportion of quartz. Rhombohedral outlines of the crystals marked (d) are suggestive of small scale dolomitization which also adds to the etch-resistance. Phase-contrast.
Fig. 8. Same as Fig. 7 but focused on the outlines of the neomorphic micrite and pseudospar crystals. Phase-contrast.

PLATE XXI

Fig. 1. Algal-bound dolo-packstone with algal-coated quartz grains. The right-hand algal-coated quartz grain shows projections of dark calcite micrite replacing the quartz. Around these dark algal micrite projections the red staining of the calcite is visible. On the left side the initial ooid lamination around the quartz grain was not destroyed by later algal coating. Treated with Alizarin Red-S. LSW 56. 80 ×. Phase-contrast.
Fig. 2. Pores in the wall of *Fusulina* sp. filled with dolomite (see the section "dolomite cement"). The filling of the chambers with dolomite seems to be dependent upon the number of pores in the wall which are filled with dolomite. The dolomite cement in the chambers shows calcitization. The two dolomite crystals in the upper right chamber are surrounded by pore-filling calcite which is only lightly stained by Alzarin Red-S because of its etch resistance due to partial silicification. Centripetal replacement of these dolomite crystals by calcite is clearly visible. Treated with Alizarin Red-S. LSW 56. 80 ×. Phase-contrast.
Fig. 3. Intra-allochem pore in a calcisphere lined with a rim of dolomite crystals (see the section "dolomite cement"). The central part of the pore was filled with clear pore-filling calcite, stained only lightly because of its etch resistance due to silicification. "Pores" in the wall of the calcisphere are vaguely visible. Treated with Alizarin Red-S. LSW 29. 200 ×. Phase-contrast.
Fig. 4. Selective dolomitization of algal pellets. The algal pellet in the lower right-hand corner has a rhombic outline indicating its dolomitization into one big dolomite crystal. Partial calcitization regenerated the original pelletal texture. Although a clotty or "grumeleuse" texture might also result from calcitization of a dolomudstone containing dolomite crystals with cloudy centers, it is evident from the depositional texture of this sample that the pellets or clots were originally algal (see the section "fabrics and textures resulting from calcitization of dolomite"). Treated with Alizarin Red-S. LSW 31. 80 ×. Phase-contrast.

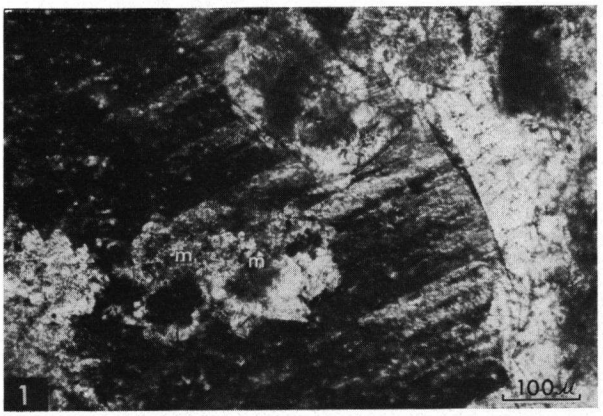
m
m
100 μ

1

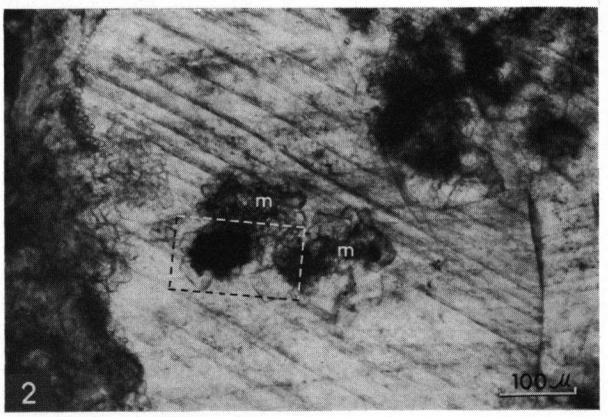
m
m
100 μ

2

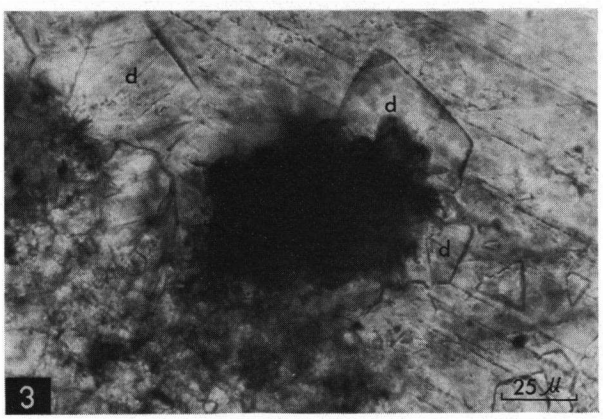
d
d
d
25 μ

3

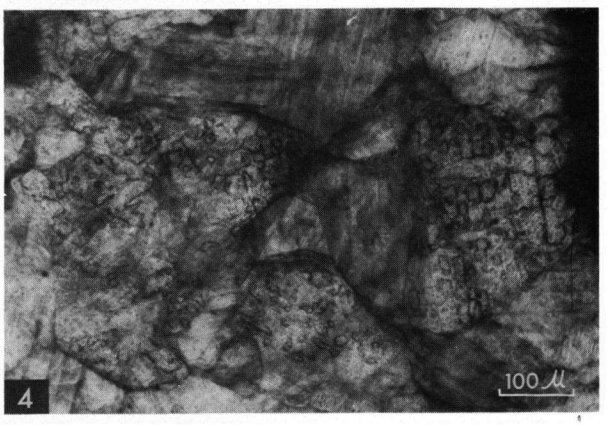
100 μ

4


25 μ

5

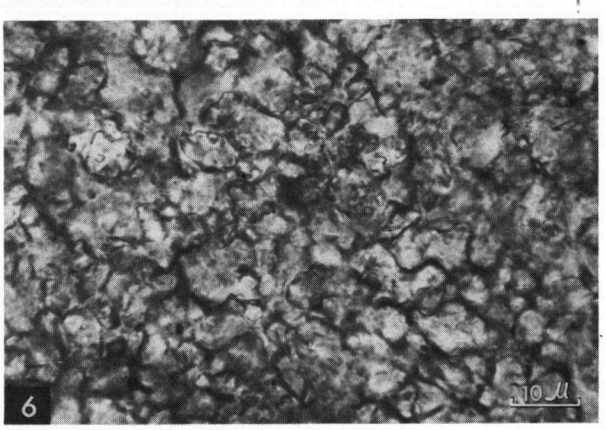
10 μ

6

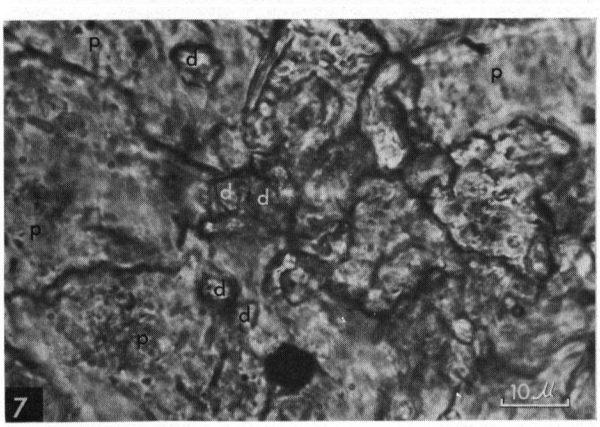
p
d
p
d
d
p
d
d
p
10 μ

7

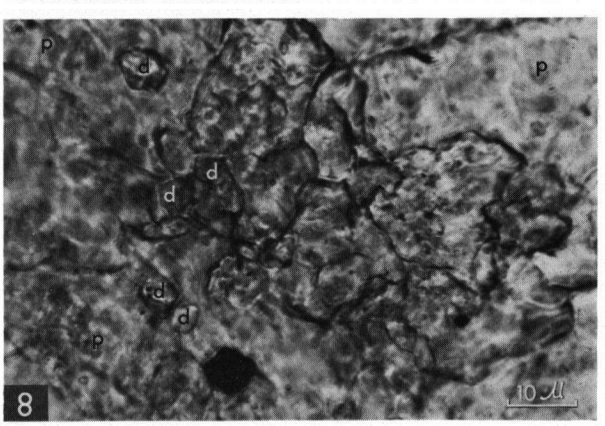
p
d
p
d
d
d
d
p
10 μ

8

Fig. 5. Intra-allochem pore of a gastropod with (1) pore-filling calcite selectively dolomitized around inclusions of an internal algal micrite coating (clearly visible in the lower left-hand corner of the figure), (2) dolomite cement (unstained zone with rhombohedral outlines), (3) calcite filling the central part of the pore space. Red staining of this central part is obscured by the effect of the phase-contrast but is visible as a red lining around the dolomite rhombohedra. See also Plate IV, Figs. 6 and 7. Treated with Alizarin Red-S. LSW 56. 80 ×. Phase-contrast.

Fig. 6. Algal pellet originally dolomitized into a rhombohedron; its dark outline can still be traced despite the obscuring effect of centripetal calcitization (see also Fig. 4). Lightly colored patches are etch-resistant due to partial silicification. Treated with Alizarin Red-S. LSW 31. 200 ×. Phase-contrast.

Fig. 7. Pressure solution seam following the path of a NW-SE fracture with evidence of recent solution by percolation of meteoric water. Transected dolomite crystals along this seam are not calcitized more intensely than elsewhere or they are not calcitized at all. Treated with Alizarin Red-S. LSW 25. 80 ×. Phase-contrast.

Fig. 8. Dissolved border of a thin section with relicts of calcitized dolomite rhombohedra. Ferric-oxide ghosts indicate the original position of the latter. Very fine quartz particles distributed in the dolomite rhombohedra appear as relicts inside the ferric-oxide ghosts. Most of the quartz particles in one former dolomite crystal show uniformity in optical orientation (dominance of yellow or blue in the 45° position). This is regarded as indicating syntaxial replacement of dolomite by quartz (see the section "replacement of dolomite"). LSW 24. 200 ×. gypsum plate. × nicols.

Fig. 9. Bryozoan with partial dolomitization of its skeleton. Calcitization of the dolomite regenerated the original fibres of the microstructure (dark vertical streaks in the upper left part of the skeleton). Treated with Alizarin Red-S. LSW 83. 200 ×. Phase-contrast.

Fig. 10. Flock of fossil non-calcareous Algae. Large filament in the upper right-hand corner is comparable to recent *Vaucheria* sp. The coherence of the flock is due to the presence of numerous tiny algal tubes. Quartz aggregates (yellow and blue) developed around remnants of originally silicified parts of the tiny tubes (see the section "source of the silica, a hypothesis"). LC 335, Peñas Pintas. 200 ×. gypsum plate. × nicols.

Fig. 11. Dolomite rhombohedra along the border of a crumbly fracture in an ultra-thin section. The calcite filling of the fracture was dissolved by the acid admixture of the coloring agent Alizarin Red-S. Partial silicification of the pore-filling calcite is evident from the residual quartz particles (blue and yellow). LSW 41. 32 ×. gypsum plate. × nicols.

Fig. 12. Detail of the center of Fig. 11. A dolomite rhombohedron is surrounded by the residual quartz particles (blue and yellow) of the dissolved, partly silicified, pore-filling calcite of the crumbly fracture. The outline of the dolomite crystal is corroded by leaching of the centripetally calcitized outer border. LSW 41. 200 ×. gypsum plate. × nicols.

Fig. 13. Euhedral quartz crystal (yellow) in a flock of fossil non-calcareous Algae. In the crystal inclusions of remnants of silicified tiny algal tubes, one is not in optical continuity (blue dot). In the upper left-hand corner is a remnant of a silicified tiny algal tube (yellow). See the section "source of the silica, a hypothesis". LSW 17. Lois Syncline West, southern flank. 400 ×. gypsum plate ⁄. × nicols.

Fig. 14. Calcitized dolomite rhombohedra enclosed in a patch of concretionary quartz. Unstained parts of the rhombohedra are silicified (see the section "calcitization of dolomite"). Treated with Alizarin Red-S. LC 233, Ciguera Synline. 200 ×. Phase-contrast.

Fig. 15. Relict rhombohedra of calcitized dolomite in pore-filling calcite. Unstained partly silicified parts of the pore-filling calcite appear dark in phase-contrast. Treated with Alizarin Red-S. LSW 68. 200 ×. Phase-contrast.

Fig. 16. Silicified algal filament in an algal flock of the insoluble residue of a recent intertidal algal mat. Awa di Oostpunt, Curaçao (Netherlands Antilles). 200 ×. gypsum plate ⁄. × nicols.

Fig. 17. Silicified felts of *Schizothrix* in an algal flock of the insoluble residue of a recent intertidal algal mat. Awa di Oostpunt, Curaçao (Netherlands Antilles). 200 ×. gypsum plate ⁄. × nicols.

Fig. 18. Silicified unicellular blue-green Algae in a patchily silicified mass of *Schizothrix*. Algal flock of the insoluble residue of a recent intertidal algal mat. Awa di Oostpunt, Curaçao (Netherlands Antilles). 200 ×. gypsum plate ⁄. × nicols.


1

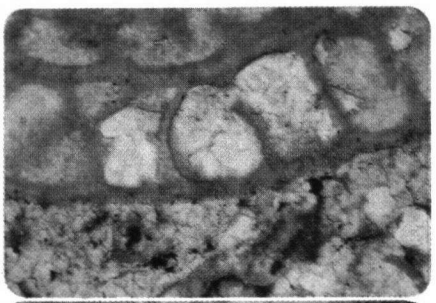
2

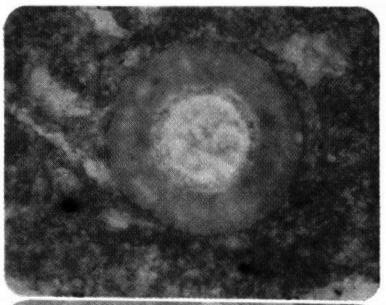
3

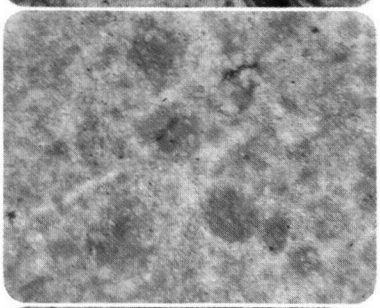
4


5

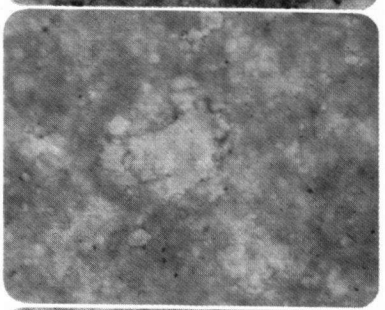
6

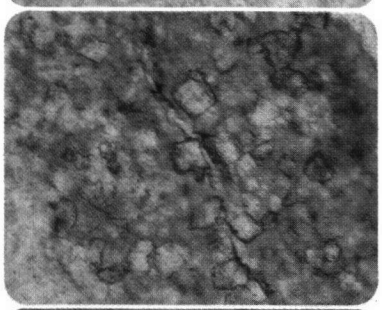
7


8


9

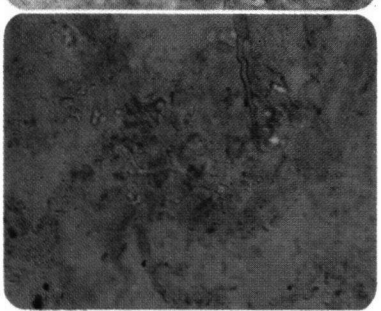
10

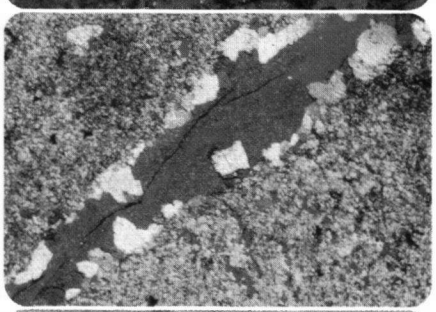
11

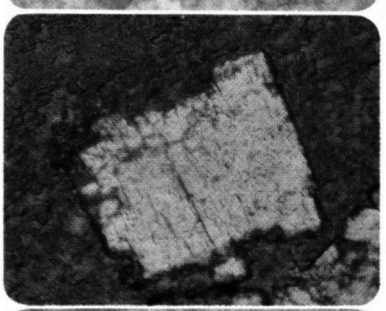
12

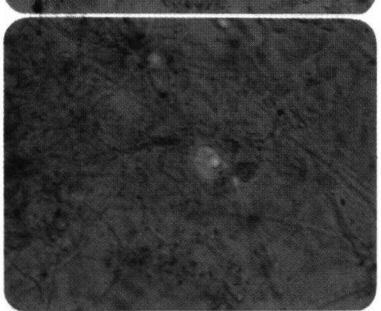
13

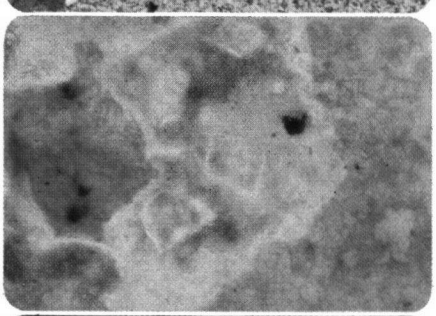
14

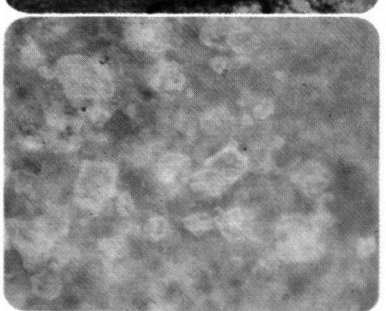
15

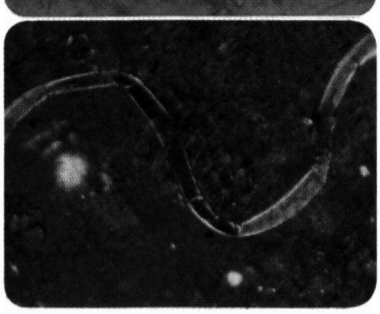
16


17

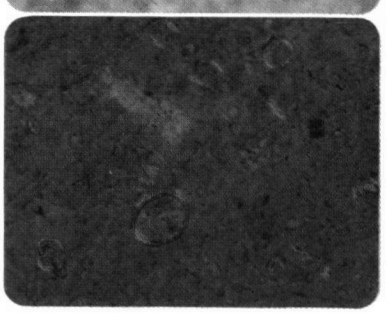
18

LOIS – CIGUERA FORMATION

section Lois Syncline West (LSW)

by J.J.de Meijer

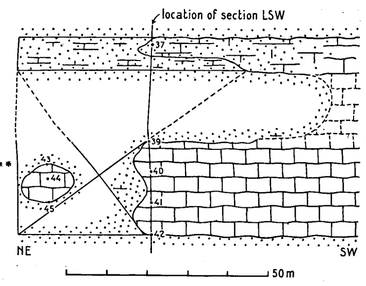

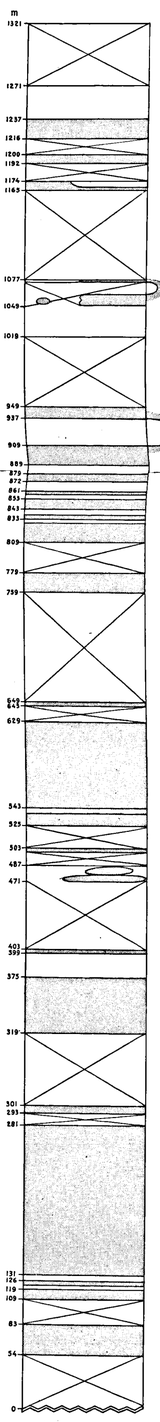

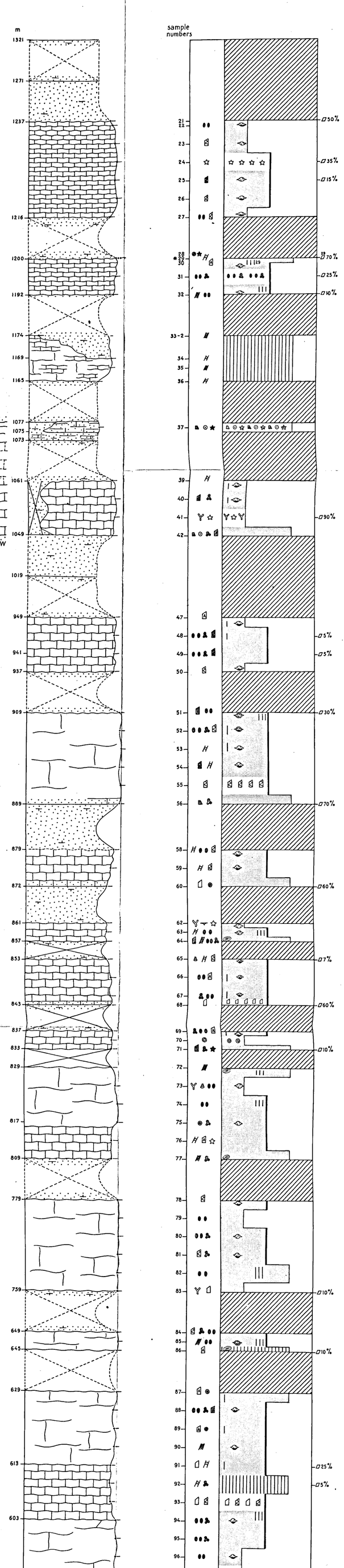

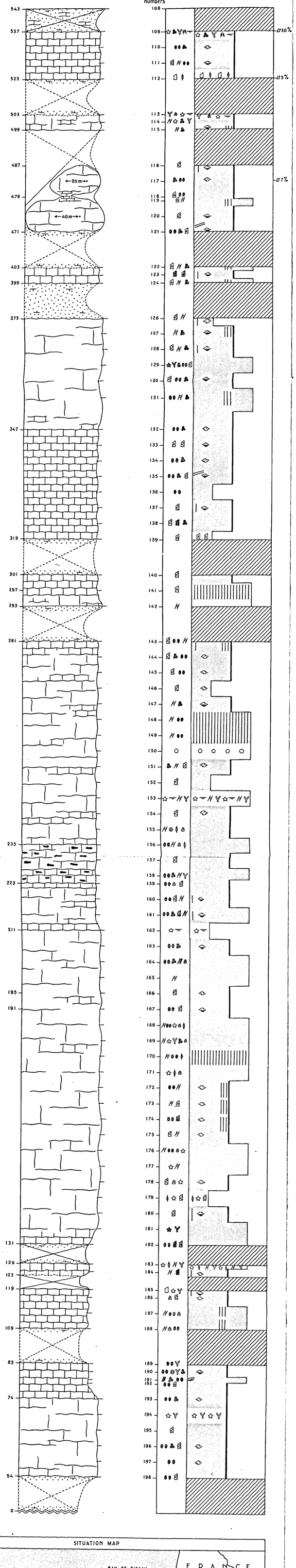

LEGEND:

LITHOLOGICAL SYMBOLS

- limestone, massive to obscurely bedded
- limestone, undulatory bedded; drawing of layering not to scale
- sandy limestone
- undulatory bedded limestone with chert nodules
- locally dolomitic undulatory bedded limestone
- quartz sandstone; silty calcareous
- calcareous sandstone
- not exposed terrigenous sediment as suggested by kind of vegetation
- not exposed terrigenous sediment as suggested by kind of vegetation; not to scale
- not exposed quartz sandstones; scattered debris between vegetation; not to scale
- not exposed quartz sandstones and limestones; scattered debris between vegetation
- not to scale
- lateral change in lithology at location of section (NE – SW)
- lateral change in lithology at location of section (NE – SW)
- lens of limestone, 20 m wide
- chert nodules
- undulatory or irregular layer contact
- linear or regular layer contact
- contact of layers hidden by vegetation
- fault

DEPOSITIONAL TEXTURE SYMBOLS

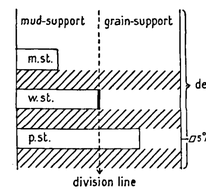

1 terrigenous sediment or not exposed sediment

2 + grain symbol — mechanically deposited limestone or limestone of which binding could not be determined

3 algal – bound, pseudostromatic limestone

4 3+ skeletal intergrowth in situ

5 3+ local skeletal intergrowth in situ

6 3+ local growth in situ

7 3+ local algalmat lamination

8 3+ oncolite

9 3+ constructed void with pore-filling calcite

10 3+ constructed void with floor of internal sediment and pore-filling calcite

11 3+ constructed void, rimmed by fibrous calcitic crust, and filled with calcite

12 3+ constructed void, rimmed by fibrous calcitic crust, and filled with internal sediment and calcite

13 3+ constructed void, floored with internal sediment, rimmed by fibrous calcitic crust and filled with calcite

GRAIN SYMBOLS

- calcareous algae
- brachiopods
- bryozoans
- calcispheres
- corals
- echinoderms
- smaller foraminifera (non fusulinids)
- fusulinids
- algal groins
- intraclasts
- algal molds
- non-algal pore-fill fossil molds
- *non-algal neomorphic fossil molds*
- ooids
- algal pellets
- quartz grains
- spherulites
- trilobites

grain symbols in gray = algally coated: ■ → algally coated pore-fill mold

* LSW 28, 29, 30, explanation see the section "relation to underlying and overlying sandstones"

** LSW 43, 44, 45, explanation see the section "signs of binding"